AMERICAN SOCIETY FOR MICROBIOLOGY | mBio®

RESEARCH ARTICLE

Rothia from the Human Nose Inhibit *Moraxella catarrhalis* Colonization with a Secreted Peptidoglycan Endopeptidase

Reed M. Stubbendieck,[a,b] Eishika Dissanayake,[c] Peter M. Burnham,[a] Susan E. Zelasko,[a,d] Mia I. Temkin,[a*] Sydney S. Wisdorf,[c] Rose F. Vrtis,[c] James E. Gern,[c,e] Cameron R. Currie[a,f]

[a]Department of Bacteriology, University of Wisconsin-Madison, Madison, Wisconsin, USA
[b]Department of Microbiology and Molecular Genetics, Oklahoma State University, Stillwater, Oklahoma, USA
[c]Department of Pediatrics, University of Wisconsin School of Medicine and Public Health, Madison, Wisconsin, USA
[d]Microbiology Doctoral Training Program, University of Wisconsin-Madison, Madison, Wisconsin, USA
[e]Department of Medicine, University of Wisconsin School of Medicine and Public Health, Madison, Wisconsin, USA
[f]David Braley Centre for Antibiotic Discovery, Department of Biochemistry and Biomedical Sciences, McMaster University, Hamilton, Ontario, Canada

ABSTRACT *Moraxella catarrhalis* is found almost exclusively within the human respiratory tract. This pathobiont is associated with ear infections and the development of respiratory illnesses, including allergies and asthma. Given the limited ecological distribution of *M. catarrhalis*, we hypothesized that we could leverage the nasal microbiomes of healthy children without *M. catarrhalis* to identify bacteria that may represent potential sources of therapeutics. *Rothia* was more abundant in the noses of healthy children compared to children with cold symptoms and *M. catarrhalis*. We cultured *Rothia* from nasal samples and determined that most isolates of *Rothia dentocariosa* and "*Rothia similmucilaginosa*" were able to fully inhibit the growth of *M. catarrhalis in vitro*, whereas isolates of *Rothia aeria* varied in their ability to inhibit *M. catarrhalis*. Using comparative genomics and proteomics, we identified a putative peptidoglycan hydrolase called secreted antigen A (SagA). This protein was present at higher relative abundance in the secreted proteomes of *R. dentocariosa* and *R. similmucilaginosa* than in those from non-inhibitory *R. aeria*, suggesting that it may be involved in *M. catarrhalis* inhibition. We produced SagA from *R. similmucilaginosa* in *Escherichia coli* and confirmed its ability to degrade *M. catarrhalis* peptidoglycan and inhibit its growth. We then demonstrated that *R. aeria* and *R. similmucilaginosa* reduced *M. catarrhalis* levels in an air-liquid interface culture model of the respiratory epithelium. Together, our results suggest that *Rothia* restricts *M. catarrhalis* colonization of the human respiratory tract *in vivo*.

IMPORTANCE *Moraxella catarrhalis* is a pathobiont of the respiratory tract, responsible for ear infections in children and wheezing illnesses in children and adults with chronic respiratory diseases. Detection of *M. catarrhalis* during wheezing episodes in early life is associated with the development of persistent asthma. There are currently no effective vaccines for *M. catarrhalis*, and most clinical isolates are resistant to the commonly prescribed antibiotics amoxicillin and penicillin. Given the limited niche of *M. catarrhalis*, we hypothesized that other nasal bacteria have evolved mechanisms to compete against *M. catarrhalis*. We found that *Rothia* are associated with the nasal microbiomes of healthy children without *Moraxella*. Next, we demonstrated that *Rothia* inhibit *M. catarrhalis in vitro* and on airway cells. We identified an enzyme produced by *Rothia* called SagA that degrades *M. catarrhalis* peptidoglycan and inhibits its growth. We suggest that *Rothia* or SagA could be developed as highly specific therapeutics against *M. catarrhalis*.

KEYWORDS asthma, acute otitis media, *Moraxella catarrhalis*, nasal microbiome, peptidoglycan endopeptidase, *Rothia aeria*, *Rothia dentocariosa*, *Rothia mucilaginosa*, *Rothia*, *asthma*

Editor Joerg Graf, University of Connecticut

Address correspondence to Reed M. Stubbendieck, stubbendieck@okstate.edu, or Cameron R. Currie, ccurrie@mcmaster.ca.

*Present address: Mia I. Temkin, Antimicrobial Defense Laboratory, The Francis Crick Institute, 1 Midland Road, NW1 1AT London, UK.

The authors declare no conflict of interest.

This article is a direct contribution from Cameron R. Currie, a Fellow of the American Academy of Microbiology, who arranged for and secured reviews by Matthew Kelly, Duke University, and Matthew Traxler, University of California, Berkeley.

Received 24 February 2023
Accepted 27 February 2023
Published 3 April 2023

The human nasal cavity is colonized by a low-diversity microbial community that includes commensals, mutualists, and opportunistic pathogens (also called "pathobionts") (1–3). Nasal pathobionts include *Staphylococcus aureus* and *Streptococcus pneumoniae* (4), which can cause disease at body sites outside the nose (e.g., blood, heart, central nervous system, and skin) (5–8). The burden that *S. aureus* and *S. pneumoniae* represent on human health has been reviewed extensively (9–14). However, in addition to these well-characterized pathobionts, the nasal cavity is also home to other potential pathogens, including *Moraxella catarrhalis*. This Gram-negative pathobiont is found almost exclusively within the human respiratory tract and is an opportunistic pathogen in children and adults with chronic respiratory diseases.

Moraxella catarrhalis is an otopathogen and is increasingly isolated as a causative agent of acute otitis media (AOM; i.e., ear infection) in children (15). Between 2008 and 2014, the rate of AOM among children in the United States remained constant (16), despite the introduction of a 13-valent pneumococcal vaccine in 2008 that demonstrably reduced the burden of AOM caused by the major otopathogen *S. pneumoniae* (17). During the same period, there was a concomitant increase from 15% to 25% in the incidence of *M. catarrhalis* isolated from children with AOM (15, 18, 19). Moreover, over 85% of clinical isolates of *M. catarrhalis* produce chromosomally encoded β-lactamases, rendering them resistant to peptidoglycan-targeting β-lactam antibiotics, including first-line empirical agents used to treat AOM (i.e., amoxicillin) (20, 21). These β-lactamases can also protect other otopathogens, including nontypeable *Haemophilus influenzae* and *S. pneumoniae*, from antibiotics in mixed-species biofilms (22–24). Furthermore, *M. catarrhalis* colonization of the nasopharynx is correlated with the development of respiratory diseases, including allergies and asthma (25, 26). For instance, in a longitudinal birth cohort study, detection of *Moraxella* during incidents of wheezing illness in the first 3 years of life was strongly associated with the development of persistent asthma in adulthood (27). Furthermore, *M. catarrhalis* is increased in respiratory secretions during acute wheezing illnesses and contributes to exacerbations of asthma and chronic obstructive pulmonary disease (COPD) (25, 28, 29). Currently, no clinical trials of vaccines for *M. catarrhalis* for children have been conducted or are ongoing. In addition, vaccines against *M. catarrhalis* for adults with COPD have not been proven to be effective at preventing disease exacerbations or stimulating a persistent immune response against this pathobiont (30–33). Given this intrinsic antibiotic resistance, the lack of vaccines, and the economic burden of these diseases, it is of interest to identify alternative therapeutics that target *M. catarrhalis*.

The human nasal cavity is a high-stress, low-resource environment (34, 35). As one means of persisting in this hostile environment, bacteria engage in competitive interspecies interactions (recently reviewed by Hardy and Merrell [36]). The competitive mechanisms that bacteria use can be broadly categorized as exploitation or interference (37). In exploitation competition, one organism prevents its competitors from accessing resources, such as nutrients or space. For instance, *Corynebacterium propinquum* from the nasal cavity produces the siderophore dehydroxynocardamine and sequesters iron from coagulase-negative staphylococci to mediate exploitation competition (38). In contrast, interference competition involves the production of toxic effectors that directly kill or inhibit the growth of competitors. As examples in the nasal cavity, *Staphylococcus lugdunensis* produces the antibiotic lugdunin to inhibit *S. aureus* (39), several *Gammaproteobacteria* species produce antimicrobial peptides with activity against *S. aureus* (40), and *Staphylococcus epidermidis* produces the antibiotic nukacin IVK45 to inhibit various bacterial species, including *M. catarrhalis* (41). In addition to antibiotics, bacteria can also use enzymes and other secreted proteins to mediate inference competition. For example, in the nasal cavity, *Corynebacterium accolens* secretes a lipase that cleaves human triacylglycerides to release short-chain fatty acids with activity against *S. pneumoniae* (42). Because *M. catarrhalis* is specialized for the human respiratory tract, we hypothesized that other bacteria which colonize the nasal cavity may have evolved mechanisms to compete with this pathobiont in its native environment. These nasal bacteria could represent an avenue for the identification of therapeutics against *M. catarrhalis*.

In this study, we characterized the nasal bacterial communities of children with and without *M. catarrhalis* colonization. Among the bacterial taxa that were more abundant in the noses of healthy children without *M. catarrhalis* colonization than in children with cold symptoms and *M. catarrhalis*, we identified *Rothia* spp. (phylum *Actinobacteria*, family *Micrococcaceae*). We isolated *Rothia* from nasal lavage samples and determined that *Rothia dentocariosa* and a potentially novel species similar to *Rothia mucilaginosa*, which we provisionally named "*Rothia similmucilaginosa*," were able to fully inhibit the growth of *M. catarrhalis* in *in vitro* coculture assays. In contrast, isolates of *Rothia aeria* were more variable in their ability to inhibit *M. catarrhalis in vitro*. Using a combination of comparative genomics and proteomics, we identified a putative peptidoglycan hydrolase called secreted antigen A (SagA). The SagA protein was present at higher relative abundance in the secreted proteomes of *R. dentocariosa* and *R. similmucilaginosa* than in those from *R. aeria*. To determine whether SagA can degrade *M. catarrhalis* peptidoglycan, we heterologously produced the protein and demonstrated its activity using zymography and against *M. catarrhalis* cultures. Finally, we showed that *R. aeria* and *R. similmucilaginosa* can protect cultures of differentiated airway epithelial cells from *M. catarrhalis* infection. Together, these data suggest that *Rothia* in the human nasal cavity may protect the host against *M. catarrhalis* colonization using the peptidoglycan endopeptidase SagA.

RESULTS

The nasal bacterial communities of healthy and children with cold symptoms and *Moraxella* colonization are distinct. We were interested in identifying commensal nasal bacteria that can inhibit the growth of *M. catarrhalis*. As a first step to identify these candidates, we compared the communities of healthy children and children with cold symptoms and PCR-confirmed *M. catarrhalis* colonization from a subset of nasal lavage specimens collected as part of the Genetic Influences on Rhinovirus-Influenced Asthma (RhinoGen) study (25, 43) (see Table S1 in the supplemental material). We extracted total DNA from specimens collected from 10 children with varying degrees of cold symptoms (median age: 7.95 years, interquartile range [IQR]: 6.6 to 8.2 years; 100% male; median cold severity score: 7, IQR: 6 to 8) and 10 children with no symptoms (median age: 8.05 years, IQR: 8 to 8.2 years; 60% male; cold severity score: 0) and used 16S rRNA gene V4 region amplicon sequencing to characterize their nasal bacterial communities. In total, we identified 235 operational taxonomic units (OTUs) at $\geq$97% sequence identity from the 20 nasal communities (Table S2). There was a slight but significant difference in the Shannon diversity index between the nasal communities isolated from healthy children (mean = 1.88, standard deviation [SD] = 0.79) and those from children exhibiting any degree of cold symptoms (mean = 1.19, SD = 0.47; Wilcoxon rank-sum test: $P = 0.029$).

To determine whether nasal bacterial community composition was associated with donor health status, we investigated beta diversity using Bray-Curtis dissimilarity and nonmetric multidimensional scaling (NMDS). In general, we found that the bacterial communities from healthy children were distinct from those from children with cold symptoms (analysis of similarity [ANOSIM] $R = 0.29$, $P = 0.0039$) (Fig. 1). However, three nasal bacterial communities from healthy children grouped with nine of the communities from children with cold symptoms. In addition, one of the bacterial communities from a child with minor symptoms (cold severity score = 4) did not group with any other community in this analysis (Fig. 1). We identified 45 bacterial OTUs with significant trends ($\alpha = 0.05$) across the ordination space (Table S2). Otu0001 ($R^2 = 0.82$, $P = 0.00001$) and Otu0222 ($R^2 = 0.51$, $P = 0.0023$), both corresponding to *Moraxella* spp., were strongly associated with communities isolated from children with cold symptoms. In contrast, we identified 24 OTUs that were associated with healthy communities. These OTUs included Otu0034 ($R^2 = 0.40$, $P = 0.024$) and Otu0039 ($R^2 = 0.34$, $P = 0.047$), which correspond to *Rothia mucilaginosa* (phylum *Actinobacteria*, family *Micrococcaceae*) and an unclassified *Rothia* sp., respectively.

***Rothia* specifically inhibit *Moraxella* species.** Given the negative correlation of *Rothia* OTUs with *Moraxella* OTUs (Fig. 1), we hypothesized that these bacteria may be able to inhibit the growth of *M. catarrhalis*. To test this hypothesis, we first isolated

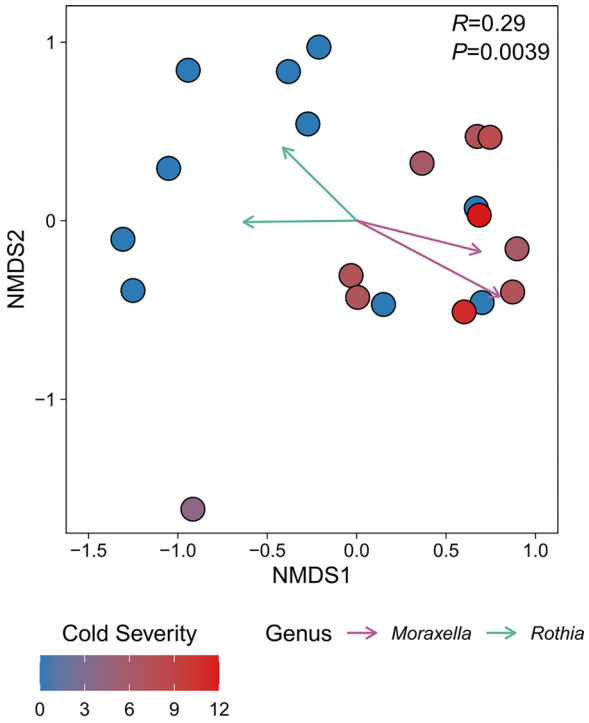

FIG 1 Bacterial community composition varies between children based on *Moraxella* colonization and correlates with cold severity. Each point in the nonmetric multidimensional scaling (NMDS) plot represents the bacterial community sequenced from one individual. Points are colored according to cold severity score (see Materials and Methods), as indicated by the key in the lower left. Vectors represent operational taxonomic units (OTUs) corresponding to either *Moraxella* or *Rothia*. Each vector originates from 0,0 and indicates a significant (α = 0.05) trend for select OTUs and their length is scaled according to the square root of their correlation coefficients such that longer vectors indicate stronger correlations. Vectors are colored by their genus-level identification, as indicated by the key in the lower right. The ANOSIM *R* and *P* values (100,000 permutations) for comparing children with upper respiratory tract infection symptoms (cold severity score $>$ 0) with healthy children (cold severity score = 0) are shown in the top right of the plot. The stress value for the NMDS plot was 0.14.

Rothia from frozen nasal lavage specimens donated as part of the RhinoGen study. In addition, we supplemented these isolates with two strains that we previously isolated from specimens donated as part of the Childhood Origins of Asthma (COAST) study (38, 44, 45).

We assessed the ability of a subset of the cultured *Rothia* isolates to inhibit the growth of *M. catarrhalis in vitro* using pairwise inhibition assays. We cultured 14 different *Rothia* isolates on brain heart infusion (BHI) agar plates. After the colonies were established, we inoculated six different *M. catarrhalis* strains next to the *Rothia* colony, then scored them for inhibition by visual assessment of the coculture after overnight incubation. Consistent with our hypothesis, we found that some *Rothia* isolates were able to inhibit the growth of multiple *M. catarrhalis* strains. In general, we did not observe differences in inhibition among different *M. catarrhalis* strains (Fig. S1). Across technical replicates of our assays, we generally observed concordance in *M. catarrhalis* inhibition. However, between different experimental replicates, *Rothia* isolates that generally inhibited *M. catarrhalis* or had no effect on its growth sometimes showed weak inhibition in another replication. Therefore, we assigned each *Rothia* isolate into one of three categories based on its average ability to inhibit *M. catarrhalis*: strong inhibition (fully inhibited most *M. catarrhalis* strains in nearly all replicates, *n* = 7), weak inhibition (partially inhibited most *M. catarrhalis* strains in nearly all replicates or had variable inhibition across replicates, *n* = 3), and no inhibition (did not inhibit most *M. catarrhalis* strains in nearly all replicates, *n* = 4) (Fig. 2A).

We then wanted to determine whether this inhibition was specific to *M. catarrhalis* or whether other *Gammaproteobacteria* were susceptible to inhibition by the *Rothia*

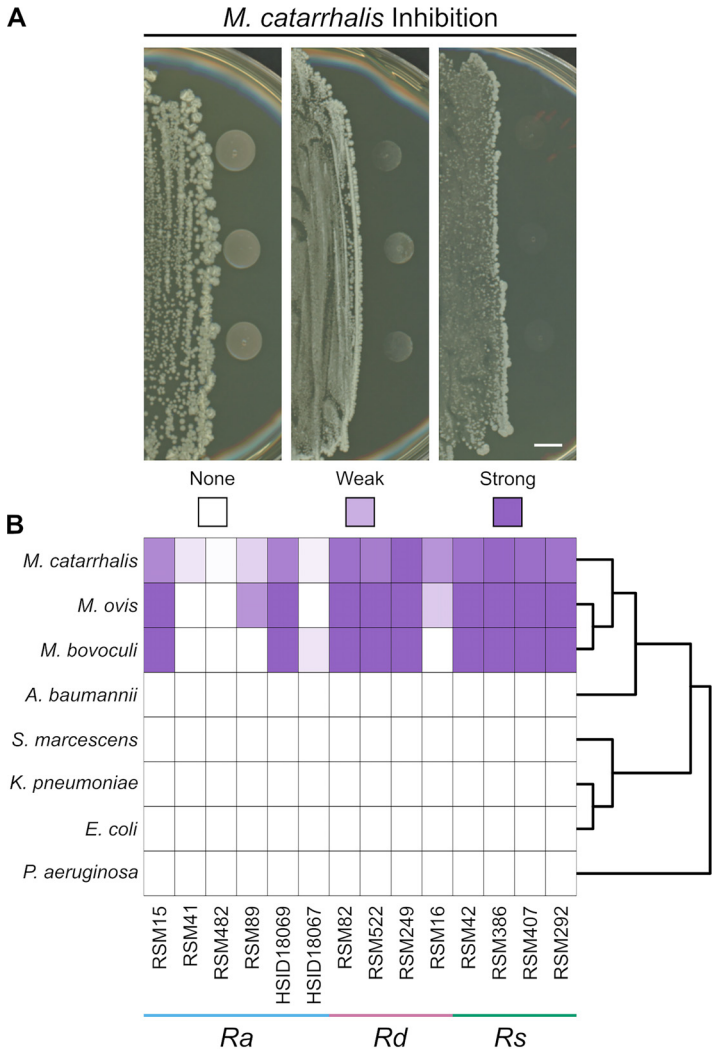

FIG 2 Inhibition of *Moraxella catarrhalis* by *Rothia*. (A) Cocultures of *Rothia* isolates (left side of image) and three colonies of *M. catarrhalis* strain O35E (right side of image) The inhibition score is indicated below each image, with the heat map key shown in panel B. Photographs were taken after co-incubation overnight on brain heart infusion (BHI) agar and are representative of ≥3 replicates. For *M. catarrhalis*, the inhibition score represents the aggregate for six different strains. See Fig. S1 for the results of each *M. catarrhalis* strain individually. Scale bar = 5 mm. (B) Heat map shows the inhibition scores of each *Gammaproteobacteria* strain (left) when paired with the corresponding *Rothia* isolate (below). Each interaction was replicated ≥3 times and the inhibition scores were averaged. Right side shows cladogram of the *Gammaproteobacteria* strains used in this study. Abbreviations: *Ra*, *R. aeria*; *Rd*, *R. dentocariosa*; *Rs*, *R. similmucilaginosa*.

isolates. We repeated the inhibition assays and included strains of *Acinetobacter baumannii*, *Escherichia coli*, *Klebsiella pneumoniae*, *Pseudomonas aeruginosa*, and *Serratia marcescens*. In addition, we tested whether these *Rothia* isolates inhibited the growth of *Moraxella bovoculi* and *Moraxella ovis*, which were isolated from a cow and sheep, respectively, with conjunctivitis (Fig. 2B). In general, we observed that all three *Moraxella* species behaved identically in the inhibition assays (i.e., if a *Rothia* isolate inhibited *M. catarrhalis*, then it also inhibited *M. bovoculi* and *M. ovis*). We never observed inhibition of a non-*Moraxella* species by any of the 14 *Rothia* isolates that we tested (Fig. 2B). These 14 *Rothia* isolates were also tested for activity against a panel containing three fungi (*Aspergillus flavus*, *Candida albicans*, and *Trichosporon asahii*), three Gram-positive bacteria (*Bacillus subtilis*, *Enterococcus faecalis*, and *S. aureus*), and one additional Gram-negative bacterium (*Enterobacter cloacae*). No inhibitory activity was observed against any fungi or bacteria, except *Moraxella* species. Taken together, these data indicate that some strains of *Rothia* produce factor(s) that specifically inhibit *Moraxella* at a distance.

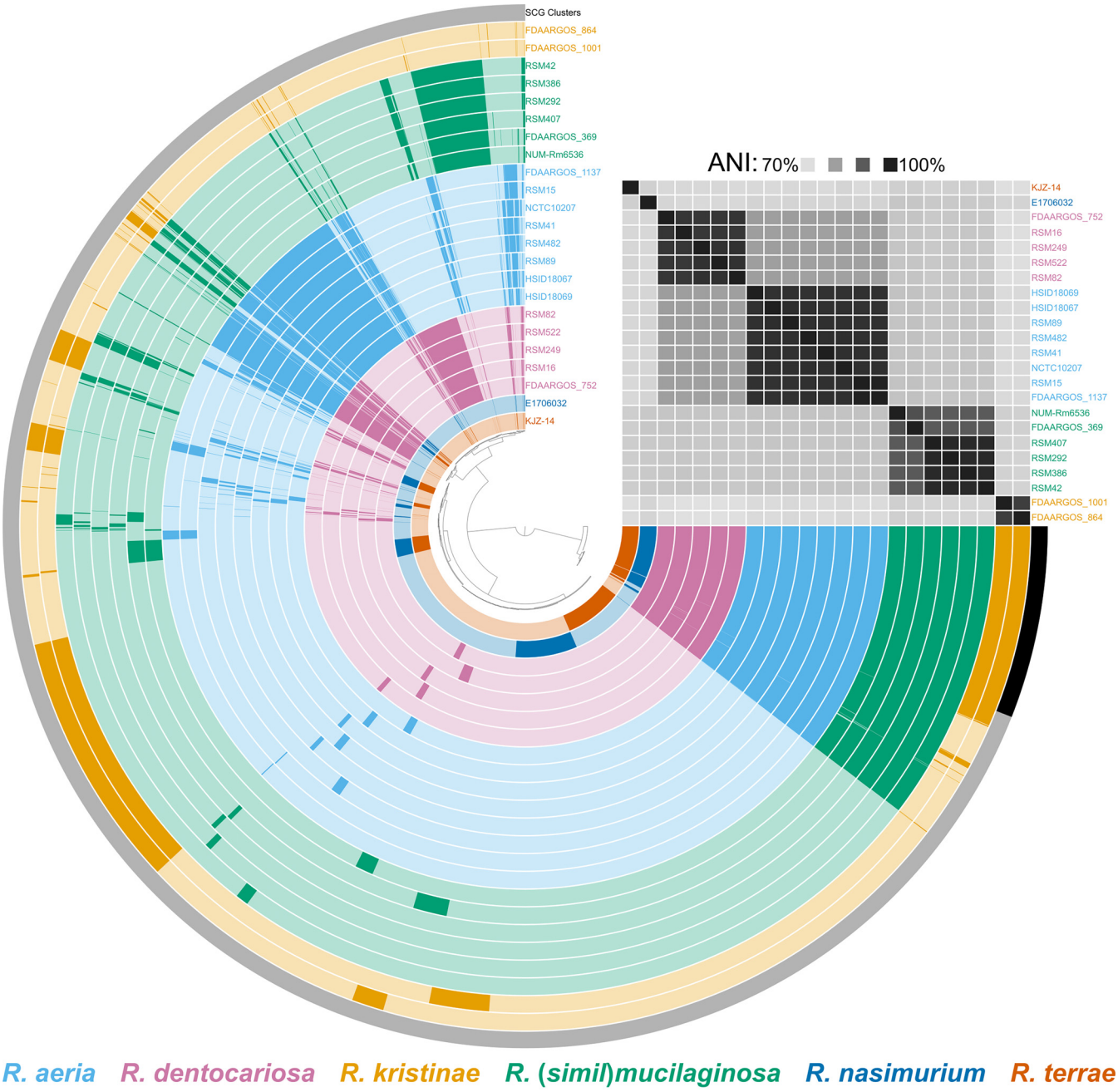

FIG 3 Pangenome of *Rothia*. This pangenome was generated from 9 reference genomes and 14 draft genome sequences of the strains used in this study using the anvi'o 7 pangenome pipeline. Each arc represents a single genome and is colored based on its species-level identification, as indicated by the key below. Genomes are ordered based on average nucleotide identity (ANI; top right). In total, this pangenome contains 48,332 genes within 8,099 gene clusters. The presence or absence of a gene cluster within a given genome is indicated by opaque and transparent colors, respectively. Black bar indicates the set of single-copy core gene (SCG) clusters.

Different species of *Rothia* are associated with inhibition and non-inhibition of *M. catarrhalis*. To confirm the identity of each *Rothia* isolate, we extracted and sequenced genomic DNA to generate draft genome sequences for each isolate used in the coculture assays. We then compared these genome sequences with 9 complete, high-quality *Rothia* genomes from GenBank, including *R. aeria*, *R. dentocariosa*, *R. kristinae*, *R. mucilaginosa*, *R. nasimurium*, and *R. terrae*. In addition, we constructed a core-genome phylogeny from 93 conserved single-copy genes using these same genome sequences. Based on gene content, average nucleotide identity (ANI), and phylogenetic placement (Fig. 3, Fig. S2), we identified the 14 *Rothia* isolates used in this study as *R. aeria* (n = 6, ANI = 97.7% to 99.5% relative to

reference strain FDAARGOS_1137), *R. dentocariosa* (n = 4, ANI = 96.5% to 96.8% relative to reference strain FDAARGOS_752), and a species closely related to *R. mucilaginosa* (n = 4, ANI: 91.5% to 91.6% relative to reference strain FDAARGOS_369). We note that though the isolates in the latter category were closely related to *R. mucilaginosa*, they did not reach the frequently used 95% ANI cutoff for species delineation (46). In addition, these four isolates did not reach this ANI threshold compared with any other characterized *Rothia* stain. Henceforth, for simplicity, we will refer to these isolates using the provisional species name "*Rothia similmucilaginosa*." A full biochemical characterization and formal classification of these *R. similmucilaginosa* isolates is forthcoming. We found that three *R. dentocariosa* isolates and all four *R. similmucilaginosa* isolates strongly inhibited *M. catarrhalis*. Two *R. aeria* isolates and one *R. dentocariosa* isolate weakly inhibited *M. catarrhalis*. The remaining four *R. aeria* isolates did not inhibit *M. catarrhalis* (Fig. 2B). We next sought to determine the identity of the anti-*Moraxella* inhibitory factor(s) produced by the inhibitory *Rothia* isolates.

Inhibition of *M. catarrhalis* by *Rothia* is not due to production of a siderophore. *Rothia* genomes contain biosynthetic gene clusters (BGCs) for the production of antibiotics and other secondary metabolites (47–49). We hypothesized that the *Rothia* strains with inhibitory activity against *M. catarrhalis* produce secondary metabolite(s) that the non-inhibitory strains lack. To test this hypothesis, we first identified BGCs contained within *Rothia* genomes using antiSMASH (50) (Fig. S3A). Consistent with a previous study that investigated the biosynthetic capacity of *Rothia* genomes (51), we identified a single BGC encoding the production of the non-ribosomal peptide siderophore enterobactin that was present in the genomes of all 14 isolates used in this study and 8 of the reference genomes (Fig. S2A). For all *R. similmucilaginosa* genomes, the enterobactin BGC was the only BGC we detected (Fig. S3A).

Siderophores are molecules produced by microbes to scavenge ferric iron and other minerals from the environment (52). In a previous study, we determined that *R. aeria* strains HSID18067 and HSID18069 did not produce siderophore activity under similar, but slightly different, assay conditions to those used in the present study (38). Here, these strains possessed no activity and partial activity against *M. catarrhalis*, respectively (Fig. 2B). Therefore, we wanted to determine if *R. dentocariosa* and *R. similmucilaginosa* strains produce siderophores as a potential mechanism to inhibit *M. catarrhalis* growth. Using chrome azurol S (CAS) assays, we detected no iron sequestration from *R. aeria* strain RSM41, *R. dentocariosa* strain RSM522, or *R. similmucilaginosa* strain RSM42 under the same conditions as used for the coculture inhibition assays (Fig. S3B), suggesting that these bacteria do not produce siderophores. In a parallel approach to test whether iron sequestration by *Rothia* is responsible for inhibition of *M. catarrhalis*, we performed inhibition assays using standard BHI agar plates $\pm$200 μM ferric chloride ($FeCl_3$). We found that iron supplementation did not appreciably change the inhibition phenotype of *M. catarrhalis* strain O35E when cultured with *R. similmucilaginosa* strain RSM42 or *R. dentocariosa* strain RSM522 (Fig. S3C). Taken together, these data indicate that iron limitation via a siderophore or production of another metabolite by *R. dentocariosa* and *R. similmucilaginosa* are not responsible for the observed inhibition of *M. catarrhalis*.

Identification of secreted proteins associated with *Rothia* strains that inhibit *M. catarrhalis*. Given the previous finding that *M. catarrhalis* inhibition was likely not due to production of enterobactin or another secondary metabolite (Fig. S3), we hypothesized that *Rothia* may produce a protein that inhibits this pathobiont.

We compared the genomes of different *Rothia* to determine whether the inhibitory strains encode proteins that were absent in the genomes of the non-inhibitory strains. When we analyzed the pangenome of *Rothia*, we determined that there was a strong signal between overall gene content and *Rothia* species-level identity (Fig. 3). Because inhibition of *M. catarrhalis* by *Rothia* occurred at a distance, we reasoned that an inhibitory protein must be secreted. Therefore, we decided to focus our subsequent analysis on genes that encode proteins with identifiable secretion signals. Of the 4,086 total groups of homologous protein-encoding genes we identified in the *Rothia* pangenomes, 488 (12% total) encoded proteins with predicted secretion signals. We observed three clusters of *Rothia* based on the presence or absence of homologous groups of genes encoding secreted

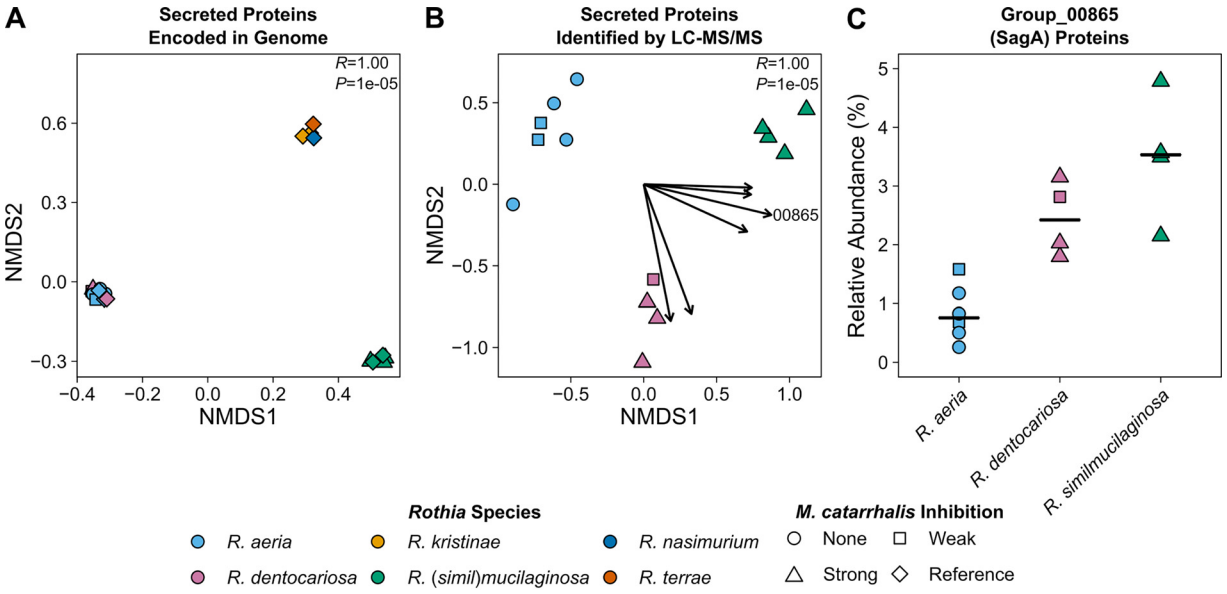

FIG 4 The secreted proteomes of *Rothia* vary by species. (A) Each point in the NMDS plot represents the presence or absence of 448 groups of homologous proteins with predicted secretion signals within a single *Rothia* genome. Points have been jittered to avoid overplotting. The ANOSIM *R* and *P* values (100,000 permutations) for comparing species are shown in the top right of the plot. The stress value for the NMDS plot was 1e–04. (B) Proteins secreted into agar by *Rothia* were extracted and identified using untargeted liquid chromatography-tandem mass spectrometry (LC-MS/MS). Each point in the NMDS plot represents the relative abundance of 181 groups of homologous proteins with predicted secretion signals detected within a single proteome. Each vector originates from 0,0 and indicates a significant (α = 0.05) trend for a subset of homologous proteins (Table 1), and their length is scaled according to the square root of their correlation coefficients such that longer vectors indicate stronger correlations. The vector for group_00865 (SagA) is labeled. The ANOSIM *R* and *P* values (100,000 permutations) for comparing species are shown in the top right of the plot. The stress value of the NMDS plot was 0.084. (C) The relative abundance of homolog group_00865, which corresponds to SagA (secreted antigen A), in the secreted proteomes of *Rothia* grouped by species. Horizontal black bars indicate the median relative abundance values. The points in all plots are colored based on the species-level identification and the shapes correspond to the *M. catarrhalis* inhibition phenotype, as indicated by the key below the plots.

proteins. The first cluster consisted of *R. aeria* and *R. dentocariosa*, the second cluster consisted of *R. kristinae*, *R. nasimurium*, and *R. terrae*, and the final cluster consisted of *R. mucilaginosa* and *R. similmucilaginosa* (Fig. 4A). These clusters are broadly consistent with *Rothia* phylogeny (Fig. S2) but did not inform the identification of a protein secreted by both *R. dentocariosa* and *R. similmucilaginosa* that inhibits *M. catarrhalis*. In addition, we did not identify any homologous groups of genes encoding secreted proteins that were universally shared between *R. dentocariosa* and *R.* (*simil*)*mucilaginosa* but were absent in *R. aeria*. Further, given that *R. aeria* strains HSID18069 and RSM15 had weak activity against *M. catarrhalis* (Fig. 2B), it is possible that these strains also produce inhibitory protein(s), albeit at lower levels.

To narrow the list of candidates for the identity of *M. catarrhalis* inhibitory protein(s), we characterized the secreted proteomes of the *Rothia* isolates that we used for inhibition assays. We cultured *R. aeria*, *R. dentocariosa*, and *R. similmucilaginosa* as before, but excised the agar near the bacterial colonies where we would inoculate *M. catarrhalis* in a coculture inhibition assay and extracted proteins. We then used untargeted liquid chromatography-tandem mass spectrometry (LC-MS/MS) to identify proteins secreted by each *Rothia* isolate. In total, we identified 181 homologous groups of secreted proteins from the three *Rothia* species. In contrast to the clustering observed when considering the content of genes encoding secreted proteins (Fig. 4A), we found that *R. aeria*, *R. dentocariosa*, and *R. similmucilaginosa* each formed their own species-based clusters (ANOSIM R = 1.00, P = 0.00001) (Fig. 4B). When we searched the secreted proteomes for proteins that were associated with both *R. dentocariosa* and *R. similmucilaginosa*, we identified six groups of homologous secreted proteins (Fig. 4B, Table 1). The proteins represented by homolog group_00865 emerged as candidates of interest for the anti-*M. catarrhalis* activity. These proteins were found in higher relative abundance in the secreted proteomes of *R. dentocariosa* (median: 2.4% of proteins with secretion signal) and *R. similmucilaginosa* (median: 3.5% of proteins

TABLE 1 Homologous protein groups associated with *R. dentocariosa* and *R. similmucilaginosa*[a]

Homolog group	Locus (name)[b]	R^2	*P*	Predicted function[c]
00865	RM6536_0976 (SagA)	0.80	0.00001	C40 family peptidase homolog
01715	RM6536_1432 (hypothetical protein)	0.74	0.00059	Plasmid partitioning protein
01164	RM6536_1002 (extracellular protease precursor)	0.74	0.0013	S8 family peptidase
01704	RM6536_0570 (hypothetical protein)	0.59	0.012	ABC transporter family substrate-binding protein
00768	RM6536_1659 (FkpA)	0.55	0.012	FKBP-type peptidyl-prolyl *cis-trans* isomerase
01276	RM6536_1518 (dihydrolipoamide acetyltransferase component)	0.55	0.013	Alpha-mannosidase

[a]The R^2 and *P* values were obtained using the envfit function from the vegan package in R. SagA, secreted antigen A.
[b]Loci and names are based on the reference genome for *R. mucilaginosa* strain NUM-Rm6536. Product names are listed if known.
[c]Predicted function was determined by BLAST search of the homolog group consensus sequence against the nonredundant protein sequences database.

with secretion signal) than in that of *R. aeria* (median: 0.75% of proteins with secretion signal) (Fig. 4C). In the *R. mucilaginosa* strain Num-Rm6536 reference genome, the gene encoding the group_00865 protein homolog is named *secreted antigen A* (*sagA*) (53). Therefore, we subsequently refer to this group of proteins as SagA proteins.

SagA proteins from *Rothia* spp. are ~20 kDa (197 to 210 amino acids), containing a 30-amino acid N-terminal signal peptide and a C-terminal endopeptidase, NlpC/P60 cysteine peptidase domain (InterPro accession no. IPR000064), and are homologous to members of the C40 peptidase family. Proteins with the NlpC/P60 domain have several known activities, including cleaving D-γ-glutamyl-meso-diaminopimelate or *N*-acetylmuramate-L-alanine linkages in peptidoglycan cross-bridges (i.e., these proteins possess peptidoglycan endopeptidase activity) (54). Based on alignment of SagA from *R. aeria* strain RSM41, *R. dentocariosa* strain RSM522, and *R. similmucilaginosa* strain RSM42 to each other and to structurally characterized C40 family peptidases, including the family type protein (MEROPS accession no. MER0001322) (55), we identified the conserved cysteine and histidine residues involved in the cysteine peptidase reaction mechanism (Fig. S4A). However, SagA is classified as a non-peptidase homolog in the MEROPS database because it has a serine (Ser-172), instead of a charged residue in the third position of the catalytic triad (Cys-His-[Asn/Gln/Glu/His]) (Fig. S4A). The charged residue does not directly participate in the reaction mechanism but is important for coordinating the basic histidine residue (corresponding to His-160 in SagA from *R. similmucilaginosa* strain RSM42). It is known that the eukaryotic endothelial protease vasohibin uses a Cys-His-Ser catalytic triad in which the serine residue orients the histidine base (56). We modeled 176 residues of SagA from *R. similmucilaginosa* strain RSM42 onto the C40 family peptidase RipA from *Mycobacterium tuberculosis* (Protein Data Bank [PDB] ID: 2XIV). Based on the homology model, we found that Ser-172 is positioned well to orient His-160 using a hydrogen bond (Fig. S4B). Therefore, we hypothesized that SagA is a functional peptidoglycan endopeptidase and may be responsible for inhibition of *M. catarrhalis* by *Rothia*.

SagA degrades peptidoglycan from *M. catarrhalis* and inhibits its growth. Currently, genetic manipulation of *Rothia* is challenging and the necessary conditions for transformation are not well-defined. Therefore, to further characterize SagA and determine its activity, we chose to use heterologous expression in *E. coli*.

We initially cloned a sequence encoding the C-terminal NlpC/P60 cysteine peptidase domain of SagA, without the N-terminal signal peptide, from *R. similmucilaginosa* strain RSM42 with an added Shine-Dalgarno sequence and start codon into an isopropyl β-D-1-thiogalactopyranoside (IPTG)-inducible expression vector. For simplicity, we subsequently refer to the truncated protein as $SagA^{37\text{-}197}$. When we sequenced three different *E. coli* clones, we identified two different 32-bp deletions of the *lac* operator sequence. Given the propensity for IPTG-inducible systems to have leaky expression (57), we hypothesized that production of $SagA^{37\text{-}197}$ in *E. coli* was cytotoxic and the deletions in the *lac* operator sequence prevented expression. Therefore, we chose to use an L-arabinose-inducible expression system, as these systems are more tightly controlled than IPTG-inducible systems (57). We confirmed dose-dependent production of the $SagA^{37\text{-}197}$ fusion protein from the L-arabinose-inducible expression system by *E. coli* as an ~17.2-kDa protein using sodium dodecyl sulfate polyacrylamide gel electrophoresis (SDS-PAGE) (Fig. S5A). During these experiments, we noticed that

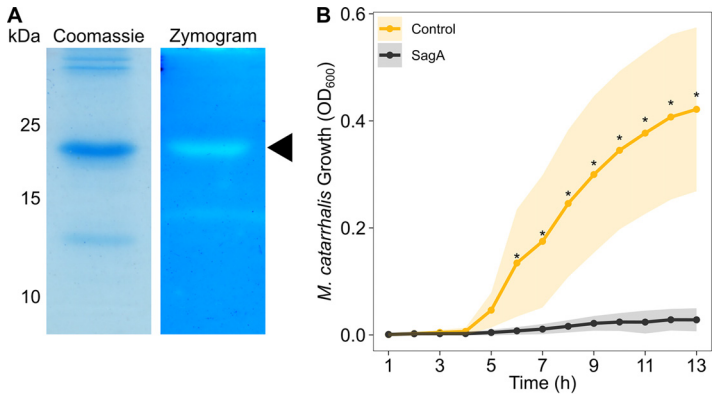

FIG 5 SagA inhibits *M. catarrhalis* through peptidoglycan degradation. (A) Two μg of partially purified 6×His-SagA$^{37\text{-}197}$ was loaded onto a standard polyacrylamide gel stained with Coomassie brilliant blue G-250 (left) or onto a zymogram gel stained with methylene blue (right). For the zymogram gel, peptidoglycan from *M. catarrhalis* strain O35E was incorporated during polymerization. Peptidoglycan degradation is indicated by clearing in the zymogram gel. Molecular weight markers in kDa are shown to the left. The 6×His-SagA$^{37\text{-}197}$ protein band is indicated with a triangle. Gels are representative of triplicate experiments. Note, the gel images were scaled to the same size. (B) Growth curve of *M. catarrhalis* strain O35E cultured for 13 h in the presence of 6×His-SagA$^{37\text{-}197}$ (black) or an equivalent extract purified from *E. coli* harboring an empty pBAD30 plasmid (gold). Each inhibition assay was repeated with four separate preparations and two technical replicates. Points represent the average optical density at 600 nm (OD_{600}) at each time point and shading indicates standard error. Asterisks (*) indicate time points at which a Wilcoxon rank-sum test demonstrated a significant difference ($\alpha = 0.05$) in growth between the control and the culture exposed to 6×His-SagA$^{37\text{-}197}$.

E. coli producing SagA$^{37\text{-}197}$ tended to grow 2 to 3× more slowly and formed smaller colonies when cultured on media containing L-arabinose, compared to uninduced controls (Fig. S5B). Taken together with the deletions observed in IPTG-inducible constructs, these data support the hypothesis that production of SagA$^{37\text{-}197}$ is cytotoxic to *E. coli*, consistent with the activity of a peptidoglycan endopeptidase.

For subsequent experiments, we chose to optimize the coding sequence for SagA for expression in *E. coli* and added a 6×His tag for purification. We partially purified SagA from *E. coli* using nickel affinity chromatography and tested the protein for peptidoglycan degradation activity using zymography. We incorporated *M. catarrhalis* strain O35E peptidoglycan into a polyacrylamide gel during polymerization. Following electrophoresis, we renatured the proteins within the zymography gel, allowed them to hydrolyze *M. catarrhalis* peptidoglycan, and stained the remaining peptidoglycan using methylene blue. We confirmed that SagA degrades *M. catarrhalis* peptidoglycan, as indicated by a zone of clearing within the zymogram gel, corresponding to the same ~19.8-kDa band in the Coomassie-stained gel (Fig. 5A). Using LC-MS/MS, we confirmed that both of these bands corresponded to 6×His-SagA$^{37\text{-}197}$.

We then wanted to determine if SagA directly inhibits *M. catarrhalis* growth. We cultured *M. catarrhalis* strain O35E in the presence of 6×His-SagA$^{37\text{-}197}$ and assessed its growth over time. We found that *M. catarrhalis* cultures exposed to SagA failed to grow, whereas cultures exposed to an equivalent purification from *E. coli* cells harboring an empty vector were not inhibited (Fig. 5B).

***Rothia* protect against *M. catarrhalis* colonization in cultures of respiratory epithelium.** To determine if *Rothia* species were protective against *M. catarrhalis* in models that are more representative of their natural environments, we chose to perform coculture assays on air-liquid interface (ALI) cultures of respiratory epithelium. We differentiated residual tissue from donor lungs into epithelial respiratory cells and colonized these cells with *R. aeria* strain RSM41, *R. dentocariosa* strain RSM522, or *R. similmucilaginosa* strain RSM42. Subsequently, we infected these cultures with *M. catarrhalis* strain O35E. After 24 h of coculture, we washed the apical surface, collected the epithelium, *Rothia*, and *M. catarrhalis* cells together, lysed the cells, and assessed *M. catarrhalis* colonization levels using a quantitative PCR (qPCR) assay. We report our results in CFU equivalents (CFUe), based on calibration of the qPCR cycle threshold with known quantities of *M. catarrhalis* in pure culture. As a control, we included a treatment where the epithelial cells were not colonized with *Rothia*.

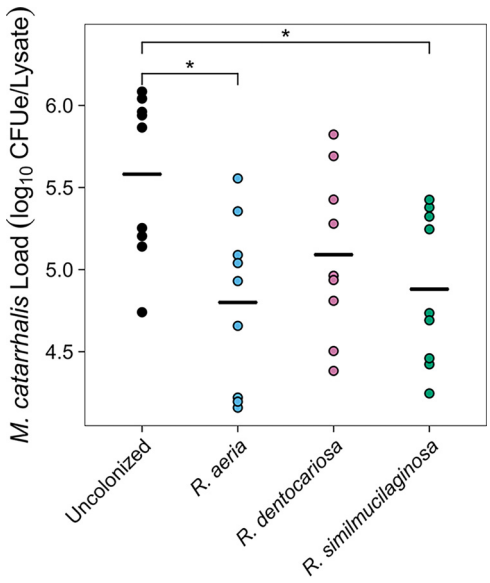

FIG 6 *Rothia* inhibit *M. catarrhalis* in respiratory epithelial cell culture. The apical surfaces of respiratory epithelial cell cultures were first colonized with *R. aeria* strain RSM41, *R. dentocariosa* strain RSM522, or *R. similmucilaginosa* strain RSM42 before subsequent infection with *M. catarrhalis* O35E. After 1 day of infection, the epithelial cells were collected and lysed, and the CFU equivalents (CFUe) of *M. catarrhalis* in each sample were quantified using quantitative PCR. Each point represents a result from a separate experiment. Horizontal black bars represent the mean abundance of *M. catarrhalis* for each treatment. Asterisks (*) indicate comparisons with significant difference (α = 0.05) after performing Tukey's honestly significant difference (HSD) tests.

We performed cocultures of *Rothia* and *M. catarrhalis* on cell lines from two different donors. There was no significant effect of cell line (analysis of variance [ANOVA] F [1,32] = 0.53, P = 0.47) or interaction between cell line and *Rothia* species (ANOVA F [3,32] = 2.55, P = 0.073) in our linear model. Therefore, we chose to consider both cell lines together for subsequent analyses. We found that there was a significant effect of *Rothia* treatment on *M. catarrhalis* strain O35E levels (ANOVA F[3,36] = 2.94, P = 0.046). However, *post hoc* comparisons did not initially reveal significant differences between any of the treatments. This non-significance was driven by a single outlying experiment in which *M. catarrhalis* strain O35E failed to colonize the cells (1.4×10^4 CFUe detected [est. <0.05% of the inoculum], compared to a median of 4.6×10^5 CFUe [est. 1.5% of the inoculum]). Consequently, we repeated our analyses with this set of experiments excluded, including the matched *Rothia*-colonized ALI cultures. As expected, we found that there was a stronger effect of *Rothia* treatment on *M. catarrhalis* strain O35E levels (ANOVA F[3,32] = 4.50, P = 0.0096). Post hoc comparisons revealed that colonization of respiratory epithelial cells with either *R. aeria* strain RSM41 (Tukey's honestly significant difference [HSD] Q = 4.72, adjusted P = 0.011) or *R. similmucilaginosa* strain RSM42 (Tukey's HSD Q = 4.24, adjusted P = 0.026) decreased *M. catarrhalis* strain O35E colonization by ~0.8 log (Fig. 6). Unexpectedly, colonization of the epithelial cells with *R. dentocariosa* strain RSM522 did not result in a decrease in *M. catarrhalis* strain O35E levels (Fig. 6).

DISCUSSION

In this study, we identified specific nasal bacteria that inhibit the growth of the pathobiont *M. catarrhalis*. We initially compared the nasal cavity bacterial communities of children with and without *Moraxella* colonization, which led us to determine that *Rothia* was associated with healthy nasal microbiomes that were free of *M. catarrhalis* colonization (Fig. 1). We performed targeted isolation of *Rothia* from nasal lavage samples. We then determined that *R. dentocariosa* and *R. similmucilaginosa* strains inhibited the growth of *M. catarrhalis in vitro*, while *R. aeria* strains tended to be less inhibitory (Fig. 2 and 3). We

reasoned that the inhibitory factor produced by these *Rothia* spp. must be a secreted protein, so we characterized the secreted proteomes of these bacteria, which led us to identify a putative endopeptidase called SagA (Fig. 4). We heterologously produced SagA and confirmed that the enzyme can degrade peptidoglycan and inhibit *M. catarrhalis* growth *in vitro* (Fig. 5). Finally, we demonstrated that *Rothia* can reduce *M. catarrhalis* levels in an airway epithelial cell model (Fig. 6).

Rothia species, including two of the three highlighted in our study, are generally considered to be inhabitants of the oral cavity (58). In a recent survey, isolates of *R. dentocariosa* and *R. mucilaginosa* were commonly cultured from pharynx samples of healthy children. However, *R. mucilaginosa* was rarely cultured from nasopharynx samples and *R. dentocariosa* was not detected at this site (59). However, we were able to culture and identify *Rothia* isolates from approximately half of the nasal lavage specimens that we tested. In addition, *Rothia* are regularly identified by sequencing studies as low-abundance members of upper and lower respiratory tract microbiomes. The relative abundances we observed were similar to what has been reported for other 16S rRNA gene amplicon sequencing studies of the anterior nares, nasal cavity, and nasopharynx (60–62). Together, these findings support the conclusion that *Rothia* are indeed bona fide inhabitants of the human nasal microbiome.

Prior research on *Rothia* has largely focused on their potential as opportunistic pathogens, primarily in immunocompromised hosts (63). However, *Rothia* have more recently been viewed as commensal bacteria and perhaps even mutualists in the oral and respiratory tracts. For instance, colonization of either an alveolar epithelial cell model or mouse lung with *R. mucilaginosa* prevented a *P. aeruginosa*-mediated, lipopolysaccharide-induced inflammatory response, resulting in reduced tissue damage compared to controls (64). Within induced sputum from individuals with bronchiectasis, the absolute abundance of *R. mucilaginosa* was inversely correlated with the levels of the proinflammatory markers interleukin 1 beta and interleukin 8 (64). The enzymatic activity of SagA itself may also trigger beneficial immune signaling in hosts. In a subcutaneous melanoma model, mice whose gastrointestinal tracts had been colonized by SagA-producing enterococci had significantly reduced tumor volume when later administered the immune checkpoint inhibitor anti-PD-L1, compared to mice treated with anti-PD-L1 alone. This antitumor effect was shown to be dependent on activation of the innate immune sensor nucleotide-binding oligomerization domain-2 (NOD2). The NOD2 sensor is activated by *N*-acetylglucosamine muramyl dipeptides generated from peptidoglycan by the D,L-endopeptidase activity of enterococcal SagA, suggesting that the microbiota can modulate responses to immunotherapy (65). In addition, NOD2 plays a role in the immune response to otitis media (66), the pulmonary immune response (67), and pathogen clearance (68). These examples, together with our findings, suggest a new role for *Rothia* as mutualists that defend against the pathobiont *M. catarrhalis* and modulate the host immune response. Subsequent work will be required to validate the role *Rothia* spp. play in these processes *in vivo*.

We do not fully understand how SagA acts on *M. catarrhalis*. In general, the outer membrane of Gram-negative bacteria, including *M. catarrhalis*, excludes molecules as large as SagA (~17.2 kDa). However, human lysozyme C (~14.7 kDa) has been previously shown to be active against *M. catarrhalis* (69). Lysozyme targets the peptidoglycan, catalyzing hydrolysis of the 1,4-beta linkages between *N*-acetylmuramic acid and *N*-acetylglucosamine residues, whereas SagA presumably uses its endopeptidase activity to target the pentapeptide stem between layers of peptidoglycan. The precise mechanism used by lysozyme to overcome the outer membrane is not fully known, but potentially involves membrane disruption through its innate cationic property at the nasal mucosal pH of 6.5 (calculated charge [*Z*] = +7.8) (70). However, unlike lysozyme, the secreted fragment of SagA is anionic at pH 6.5 (calculated *Z* = –3.2). Perhaps *Rothia* produce their own cationic peptides that act to permeabilize the outer membrane to SagA, or take advantage of a host-produced protein *in vivo*. In the latter case, one such possibility is lactoferrin, which is known to permeabilize the outer membrane of Gram-negative bacteria (71) and is present at high concentrations within nasal secretions (72). Therefore,

further work is required to determine how SagA gains access to the peptidoglycan of *M. catarrhalis*. Moreover, additional work is necessary to determine why *Moraxella* species were more susceptible to inhibition by *Rothia* than any of the other bacteria that we tested, including other closely related *Gammaproteobacteria*.

Here, we note an inconsistency between our *in vitro* and ALI cell culture results. We found that *R. aeria* tended to be non-inhibitory toward *M. catarrhalis in vitro*. However, *R. aeria* strain RSM41, which we chose as a representative of this species because it almost never inhibited *M. catarrhalis* in inhibition assays, was equally protective against *M. catarrhalis* as *R. similmucilaginosa* in ALI cell cultures. Although *R. aeria* tended to secrete less SagA than *R. dentocariosa* and *R. mucilaginosa*, it is possible that *R. aeria* produces sufficient quantities of the enzyme when cultured on epithelial cells, the anti-*M. catarrhalis* activity of SagA is potentiated by a host-produced factor (see above), or *Rothia* produces additional proteins that are responsible for *M. catarrhalis* inhibition on cells.

In conclusion, we report that *Rothia* species potentially inhibit colonization of the nasal cavity by *M. catarrhalis* using an interference competition mechanism by producing a secreted peptidoglycan endopeptidase that directly inhibits *M. catarrhalis* growth. Given the specificity of these *Rothia* against *Moraxella* spp., we suggest that these bacteria or SagA itself could be developed as therapeutics to selectively inhibit nasal colonization by *M. catarrhalis*. Furthermore, we suspect that additional efforts to screen the nasal microbiota for bacteria that produce antimicrobials will yield more examples of proteins or metabolites with anti-*M. catarrhalis* activity.

MATERIALS AND METHODS

Nasal specimen collection and cold severity scoring. The nasal lavage specimens used in this study were collected from children and banked as part of the RhinoGen study (25, 43). Informed consent was obtained from guardians, and the Human Subjects Committee at the University of Wisconsin-Madison approved the study (institutional review board [IRB] approval no. H-2007-0136-CR008). The cold severity score was determined after sample collection. This score is the summation of daily symptom scores for the period of the illness. Specimens collected within $\pm$3 days of illness symptoms were considered to be associated with that illness. The daily scores ranged from 0 for absent to 3 for severe respiratory symptoms (25) (Table S1).

DNA extraction and 16S rRNA gene V4 region amplicon sequencing. We extracted total DNA from nasal lavage samples using the Bacteremia DNA isolation kit (MO BIO Laboratories Inc.). We included a negative extraction control of sterile water treated identically to the samples. All samples were quantified using a Qubit fluorometer with broad range standards (Invitrogen). Initially, we attempted to directly amplify the 16S rRNA gene V4 region from the extracted total DNA. However, we did not observe amplification after electrophoresis of PCR products on a 1% (wt/vol) agarose Tris-acetate-EDTA (TAE) gel. Therefore, we decided to use a nested PCR approach.

We first amplified the near full-length 16S *rRNA* gene in triplicate from the extracted samples with primers 27F (5′-AGAGTTTGATCCTGGCTCAG-3′) and 1492R (5′-GGTTACCTTGTTACGACTT-3′) using KAPA HiFi HotStart DNA polymerase (Roche). Each 25-μL reaction mixture contained 5 μL of extracted DNA (median: 34 ng, IQR: 3.8 to 110 ng) and 20 pmol of each primer. We used the following PCR cycling conditions: 95°C for 1 min; 15 cycles of 95°C for 30 s, 58°C for 30 s, and 72°C for 30 s; and a final extension at 72°C for 5 min. Subsequently, we amplified the 16S *rRNA* gene V4 region in triplicate using the PCR products as the template with primers 515F (5′-[P5 Illumina Adapter]-[Index]-TATGGTAATTGTGTGCCAGCMGCCGCGG TAA-3′) and 806R (5′-[P7 Illumina Adapter]-[Index]-AGTCAGTCAGCCGGACTACHVGGGTWTCTAAT-3′). Each 25-μL reaction mixture contained 2 μL of the unpurified first-round PCR product and 10 pmol of each primer. We used the same PCR cycling conditions as above. We electrophoresed 45 μL of pooled triplicated second-round PCR products on a 1.2% (wt/vol) agarose 0.5$\times$ Tris-borate-EDTA (TBE) gel at 100 V for 1 h. Next, we purified the PCR product from the agarose gel using the Wizard SV Gel and PCR Clean-Up System (Promega). We quantified DNA as described above. In the negative extraction control, the DNA concentration was below the limit of detection. We pooled 2 ng of each sample together with 1 μL of the undiluted negative extraction control. The amplicon libraries were prepared and sequenced using the 2$\times$ 300-bp paired-end Illumina MiSeq platform at the University of Wisconsin-Madison Biotechnology Center (Madison, WI).

Bacterial community analysis. We used fastp version 0.20.0 (73) for quality control and preprocessing of the raw amplicon sequencing reads. We used the mothur version 1.44.1 pipeline (74) for read processing, assembly, alignment, and classification. For sequence classification, we used the expanded human oral microbiome database 16S *rRNA* RefSeq version 15.1 (3). We defined OTUs using a 97% sequence similarity threshold (Table S2). There was $>$99% coverage of these samples, as assessed by Good's Coverage Metric (Table S1). For all subsequent analyses, we used R version 4.0.4 (75). We processed the OTU table generated by mothur and subtracted the reads from each OTU in each sample corresponding to the number of reads detected in the negative extraction control. If OTU counts became negative after subtraction, we replaced the negative value with 0. We removed OTUs represented by $<$10 total reads from the data set. We then converted OTU counts to relative abundances and used the phyloseq package version 1.33.0 (76) and the vegan package version 2.5–

6 (77) in R to perform NMDS and ANOSIM based on the Bray-Curtis dissimilarity between nasal bacterial communities. We used the envfit function from vegan to fit OTU vectors onto the ordination plot.

Bacterial isolation, culturing, and initial identification. To obtain isolates for culture-based work, we diluted 200 μL of thawed nasal lavage specimens with 800 μL of sterile phosphate-buffered saline (PBS) and then inoculated 100 μL onto 25-mL BHI (DOT Scientific) plates (diameter: 8.6 cm) solidified with 1.5% [wt/vol] agar (VWR). In addition to using standard BHI plates, we also included plates with 50 μg/mL lithium mupirocin (Sigma-Aldrich) to inhibit the growth of *Staphylococcus* spp. and allow for isolation of slower-growing organisms and 25 μg/mL vancomycin (Sigma-Aldrich) to inhibit the growth of Gram-positive bacteria and enrich for *M. catarrhalis*. Each sample was plated in triplicate onto both medium types. We incubated plates aerobically at 37°C for 1 week. We selected ≥2 colonies of each distinct morphotype per plate and passaged the isolates aerobically on BHI plates with no antibiotic supplementation at 37°C until we obtained pure cultures. All bacterial isolates were cryopreserved at −80°C in 25% (vol/vol) glycerol. Bacterial strains used in this study are listed in Table S3 in the supplemental material. For routine culturing and all following assays, we used BBL BHI (Becton, Dickinson and Co. [BD]) solidified with 1.5% (wt/vol) Bacto agar (BD) for plates because we observed poor or inconsistent growth of *M. catarrhalis* on BHI or agar produced by other manufacturers. For experiments testing the effect of iron on inhibition, we supplemented the BHI agar plates with 200 μM $FeCl_3$ (Fisher Scientific).

To identify isolates to the genus level, we performed colony PCR using the universal 27F (5′-AGAGTTTGATCMTGGCTCAG-3′) and 1,492R (5′-CGGTTACCTTGTTACGACTT-3′) primers (78). Briefly, we suspended a small portion of each bacterial colony or liquid culture in 20 μL of 0.02 N sodium hydroxide and incubated the samples at 95°C for 10 min. We then chilled the samples on ice and centrifuged them at 21,130 × *g* for 5 min and used 1 μL of the supernatant as the template for PCR. We sequenced the PCR products using the Sanger method at the University of Wisconsin Biotechnology Center DNA Sequencing Facility (Madison, WI) and identified isolates to the genus level with the Ribosomal Database Project Classifier (79).

Inhibition assays. To determine whether *Rothia* isolates inhibited *M. catarrhalis* and other *Gammaproteobacteria*, we used coculture plate inhibition assays. We inoculated 3 mL BHI broth with single colonies of *Rothia* from 2-day-old plates and incubated the cultures at 37°C while shaking. After overnight growth, we diluted each culture to an optical density at 600 nm (OD_{600}) of 0.05 in 3 mL fresh BHI, incubated the cultures until they reached an OD_{600} of 0.4 to 0.6, and spread 50 μL in a ~6 × ~2 cm-wide line in the center of a 25-mL BHI agar plate (diameter: 8.6 cm). We incubated the plates aerobically for 3 days at 37°C. We prepared overnight cultures of *M. catarrhalis* and other *Gammaproteobacteria* by inoculating single colonies into 3 mL BHI broth and incubated the cultures at 37°C with shaking. After overnight growth, we diluted the cultures to an OD_{600} of 0.5 in fresh BHI and spotted 5 μL approximately 0.5 cm away from the line of *Rothia*. When the spots dried, we returned the plates to 37°C, then scored them for inhibition after overnight incubation. All inhibition assays were experimentally replicated ≥3 times, with at least 2 technical replicates per experiment.

Genomic DNA extraction and sequencing. We used either the DNA Miniprep kit (ZymoBIOMICS) with 2× 5-min bead beating steps or the MasterPure Yeast DNA purification kit (Lucigen) with the addition of 1 μL Ready-Lyse Lysozyme Solution (Lucigen) and 1 μL 5 mg/mL RNase A (Lucigen) to lyse *Rothia* isolates and purify genomic DNA. Libraries were prepared with a single library preparation method based on the Illumina Nextera kit and sequenced using the 2× 150-bp paired-end Illumina NextSeq 2000 platform at SeqCenter (Pittsburgh, PA).

Genome assembly and annotation. We processed raw genomic reads using fastp 0.20.0 and assembled draft genome sequences using SPAdes 3.11.1 (80), using default parameters for both. To identify homologues present across *Rothia* genomes, we downloaded high-quality complete genome sequences of *R. aeria*, *R. dentocariosa*, *R. kristinae*, *R. mucilaginosa*, *R. nasimurium*, and *R. terrae* from GenBank. We identified protein-coding genes with Prokka (81) using default parameters and used BuildGroups.py from PyParanoid (82) to build groups of homologous gene families. To predict secreted proteins, we submitted the consensus sequences for each homologous family identified by PyParanoid to the SignalP-5.0 webserver (https://services.healthtech.dtu.dk/service.php?SignalP-5.0) (83).

Pangenome analysis. To generate a pangenome, we used the anvi'o 7 pangenome analysis pipeline (84) with the following parameters: --minbit 0.5 --mcl-inflation 10 --use-ncbi-blast.

Core-genome phylogeny. We constructed a core-genome phylogeny of nasal *Rothia* isolates using core_species_tree.pl (https://github.com/chevrm/core_species_tree) as previously described (85). We used FigTree v1.4.3 (https://github.com/rambaut/figtree/) to root the phylogeny on *Kocuria rosea* ATCC 186 and display the branch length based on proportional length to the root.

Detection and identification of *Rothia* BGCs. We identified BGCs in *Rothia* genomes using antiSMASH version 4.2.0 (50) with the following parameters: --clusterblast --knownclusterblast --smcogs. To identify relationships between the *Rothia* BGCs, we used BiG-SCAPE 1.0.1 (86) with the following parameters: --cutoffs 0.3 --include_singletons. We generated a presence-absence matrix of BGCs in *Rothia* using the clustering families identified by BiG-SCAPE.

CAS assay. We used the overlay CAS assay to test for siderophore production as previously described (87). We cultured *Rothia* for 3 days at 37°C, as above. We then overlaid each plate with 5 mL of CAS reagent overlay (52.5 μM CAS, 50 μM $FeCl_3$, 0.5 mM hexadecyltrimethylammonium bromide, 10 mM piperazine-N, N′-bis[2-ethanesulfonic acid], 1% [wt/vol] agarose [pH 6.8]) (88) and incubated the plates at ambient temperature in the dark for 4 h before scanning them for color change, which would indicate the production of a siderophore (89).

Extraction of secreted proteins. To identify proteins secreted by *Rothia* isolates into agar, we adapted a previously used protocol (90). We cultured *Rothia* onto six 25-mL BHI plates, as above. After

incubation for 3 days at 37°C, we used clean razor blades to excise the agar from a distance of ~0.1 to ~1 cm away from both sides of the *Rothia* without disturbing the bacterial colony.

We centrifuged the agar slices at 4,000 × *g* for 10 min at ambient temperature, then combined them with an equal volume of extraction buffer (50 mM Tris-HCl, 0.2% [wt/vol] *N*-lauroylsarcosine sodium salt [pH 7.5]) and incubated the mixture at ambient temperature on a shaking platform set at 250 rpm overnight. We then centrifuged the samples at 4,000 × *g* for 20 min at ambient temperature and filtered the supernatant through cheesecloth to remove agar. We added trichloroacetic acid (TCA) to a final concentration of 7.5% (wt/vol) and precipitated protein overnight at −20°C. We pelleted the precipitated protein by centrifuging the samples at 4,000 × *g* for 30 min at 4°C. We then washed the protein pellet three times with 1 mL acetone and centrifugation at 21,130 × *g* for 5 min at 4°C. We evaporated residual acetone under a laminar flow hood. To remove residual agar from the samples, we first resuspended the protein pellets in 250 μL of 50 mM Tris-HCl (pH 7.5) and centrifuged the samples at 21,130 × *g* for 30 min at 4°C. We then transferred the supernatant into a new tube, and centrifuged the samples overnight at 21,130 × *g* at 4°C. Finally, the supernatant was transferred into a new tube and protein content was measured using a Coomassie protein assay (Thermo Fisher Scientific). We analyzed 3 μg of each protein sample by SDS-PAGE using a 12% Criterion TGX precast midi protein gel. We visualized proteins by staining with RAPIDstrain (G-Biosciences) for 1 h followed by 3× 15-min destaining washes in distilled water.

Identification of secreted proteins. We submitted protein samples for digestion and LC-MS/MS analysis at the University of Wisconsin Biotechnology Center Mass Spectrometry Facility (Madison, WI). To precipitate proteins, 60 μL of each sample was treated with a mixture of 10% TCA/50% acetone/40% water (vol/vol/vol) for 30 min on ice. The samples were centrifuged at 16,000 × *g* for 10 min and the pellet was washed with 800 μL acetone at −20°C. The samples were then centrifuged as described above and washed with 800 μL acetone at −20°C. Subsequently, the pellets were resolubilized and denatured in 50 μL of a solution containing 8 M urea, 50 mM ammonium bicarbonate (NH_4HCO_3), and 1 mM Tris-HCl (pH 8.5), then sonicated for 1 min. The proteins were quantified from 10 μL of the sample with the Pierce 660 nm Protein Assay reagent. The remainder of the sample was reduced by combining it with 5 μL of 25 mM dithiothreitol (DTT), 10 μL of methanol, and 65 μL of NH_4HCO_3 (pH 8.5). The samples were incubated at 52°C for 15 min, then cooled on ice before being alkylated with 6 μL of 55 mM chloroacetamide for 15 min in the darkness at ambient temperature. The alkylation reaction was quenched with 16 μL of 25 mM DTT. To digest the proteins, 14 μL of a trypsin/LysC solution (100 ng/μL of 1:1 trypsin [Promega] and LysC [FujiFilm] mix in 25 mM NH_4HCO_3) and 44 μL of 25 mM NH_4HCO_3 (pH 8.5) was added to the samples and incubated for 2 h at 42°C. Afterwards, 7 μL of the trypsin/LysC solution was added to the samples and digestion continued at 37°C overnight. The digestion reaction was terminated by addition of trifluoroacetic acid (TFA) to a final concentration of 0.3% [vol/vol].

The digested and acidified samples were cleaned using OMIX C18 SPE cartridges (Agilent) following the manufacturer's protocol, eluted with 20 μL of 50% (vol/vol) acetonitrile (ACN) with 0.1% (vol/vol) TFA, dried, and reconstituted in 40 μL 2% (vol/vol) ACN with 0.1% (vol/vol) formic acid. Peptides were analyzed by nanoLC-MS/MS using the Agilent 1100 nanoflow system (Agilent) connected to an LTQ-Orbitrap Elite (Thermo Fisher Scientific) equipped with an EASY-Spray electrospray source (held at constant 35°C). Chromatography of peptides prior to mass spectral analysis was accomplished using a capillary emitter column (PepMap C18, 3 μM, 100 Å, 150 × 0.075 mm, Thermo Fisher Scientific) onto which 2 μL of the extracted peptides was automatically loaded. A NanoHPLC (high-performance liquid chromatography) system delivered 0.1% (vol/vol) formic acid (Solvent A), and 99.9% (vol/vol) ACN with 0.1% (vol/vol) formic acid (Solvent B) at a flow rate of 0.50 μL/min to load the peptides over a 30-min period. The flow rate was adjusted to 0.3 μL/min to elute peptides directly into the nano-electrospray with a gradual gradient of 0% to 30% B over 78 min and concluded with a 5-min fast gradient from 30% to 50% Bm at which time a 5-min flash-out from 50% to 95% B took place. As peptides eluted from the HPLC column/electrospray source survey, MS scans were acquired in the Orbitrap at a resolution of 120,000, followed by CID-type MS/MS fragmentation of the 30 most intense peptides detected in the MS scan from 350 to 1,500 *m/z*. Redundancy was limited by dynamic exclusion.

The raw MS/MS data files were converted to the mgf file format using MSConvert (ProteoWizard) and searched against user-defined databases for each *Rothia* strain along with a cRAP common lab contaminant database using in-house Mascot search engine version 2.7.0 (Matrix Science) with variable methionine oxidation plus asparagine or glutamine deamidation and fixed cysteine carbamidomethylation. The peptide mass tolerance was set at 10 ppm and fragment mass at 0.6 Da. Protein annotations, significance of identification, and spectral-based quantification was determined with Scaffold version 4.11.0 (Proteome Software Inc.). The protein identifications were accepted if they could achieve a false discovery rate of <1.0% and contained at least 3 identified peptides. Protein probabilities were assigned by the Protein Prophet algorithm (91). Proteins that contained similar peptides and could not be differentiated based on MS/MS alone were grouped to satisfy the principles of parsimony. Proteins which shared significant peptide evidence were grouped into clusters.

Comparison of secreted proteomes. We mapped the spectral counts for each protein identified by LC-MS/MS onto the homolog groups generated using PyParanoid described above. In cases where we identified multiple proteins within the same homolog group from the same strain, we aggregated the spectral counts into a single count for that homolog group. We transformed spectral counts into a relative abundance by dividing each count by the total number of spectral counts identified in a sample. We then filtered out groups of potentially contaminating cytoplasmic proteins based on the presence of a signal peptide as determined by SignalP. We used the phyloseq and vegan packages in R to perform NMDS and ANOSIM and to fit homolog group vectors onto the ordination plot as above.

SagA sequence alignment. We aligned the primary sequences of SagA from *R. aeria* strain RSM41, *R. dentocariosa* strain RSM522, and *R. similmucilaginosa* strain RSM42 against structurally characterized C40 family peptidase homologues using MEGA X (92). We visualized the alignment using the ggmsa package (93) in R.

SagA structure modeling. We used the Phyre2 webserver (http://www.sbg.bio.ic.ac.uk/phyre2/) (94) to generate a structure of SagA by modeling 176 amino acids (89% of the primary sequence) from *R. similmucilaginosa* onto the hypothetical invasion protein of *M. tuberculosis* (PDB ID: 2XIV). We visualized this structural model using PyMol version 2.5.0 (95).

Generating *sagA* constructs. For initial experiments, we cloned *sagA* from *R. similmucilaginosa* strain RSM42 using primers oRSC91 (5′-AGGAGGAATTAACTATGGATCTGTCCTACGACTACACC-3′) and oRSC92 (5′-CCGCCAAAACAGCCAAGCTTTTAGAGAGCGGTGTAGTAGC-3′) and the vector pBAD30 using primers oRSC93 (5′-AAGCTTGGCTGTTTTGGCGG-3′) and oRSC94 (5′-CATAGTTAATTCCTCCTGAATTCGCTAGCCCAAAAAAACG-3′). These primers contained overhangs for assembly and included an optimal *E. coli* Shine Dalgarno sequence. We combined these fragments together using Gibson assembly (96) and transformed the products into the chemically competent *E. coli* strain NEB 5α to generate strain RSC0026. For subsequent experiments, we ordered a codon-optimized *sagA* sequence with an in-frame coding sequence for an N-terminal 6×His tag as a single gene block (GenScript). We amplified this gene block using primers oRSC130 (5′-ATGCGAATTCAG GAGGTCATCATGCACCATCATCATCACCATGA-3′) and oRSC131 (5′-ATGCAAGCTTTCAGAGGGCGGTGTAATACC-3′). These primers contained overhangs with an optimal *E. coli* Shine Dalgarno sequence and restriction sites for EcoRI and HindIII, respectively. We cloned the digested gene block into pBAD30 using EcoRI and HindIII (New England Biolabs) and transformed the product into the chemically competent *E. coli* strain Top10 to generate strain RSC0060. All plasmids were validated using whole plasmid sequencing at plasmidsaurus (Eugene, OR).

Heterologous production and purification of SagA$^{37\text{-}197}$. We inoculated 250 mL of terrific broth (2.4% [wt/vol] yeast extract, 2% [wt/vol] tryptone, 0.4% [vol/vol] glycerol, 17 mM KH_2PO_4, 72 mM K_2HPO_4) with 250 μL of an overnight culture of *E. coli* strain RSC0060 and incubated the culture at 37°C while shaking at 250 rpm. When the cultures reached an OD_{600} of 0.1, we induced production of 6×His-SagA$^{37\text{-}197}$ with a final concentration of 0.2% (wt/vol) L-arabinose, then continued incubation while shaking for 24 h. Subsequently, we collected the cells by centrifugation at 4,000 × *g* at 4°C for 30 min. We partially purified 6×His-SagA$^{37\text{-}197}$ from the cell pellet using a Ni-NTA Fast Start kit (Qiagen) following the manufacturer's protocol under native conditions, with the addition of lysis by sonication.

Zymography assay. To prepare the substrate for zymography, we inoculated 500 mL BHI with 1 mL of a *M. catarrhalis* overnight culture and incubated the cultures at 37°C while shaking. When the cultures reached an OD_{600} of 1.0, we collected the cells by centrifugation at 4,000 × *g* at 4°C for 30 min. We resuspended the cell pellets in 50 mL wash buffer (20 mM Tris-HCl, 100 mM NaCl [pH 7.5]). We then centrifuged the cell suspensions as described above, resuspended them in 10 mL of 1.5 M Tris-HCl (pH 8.8), and stored 1-mL aliquots at −20°C until use. We prepared gels with standard protocols using the Laemmli buffer system, with gels containing 20% (wt/vol) polyacrylamide in the resolving gel and 4% (wt/vol) polyacrylamide in the stacking gel. For zymography gels, during polymerization we incorporated *M. catarrhalis* cells which had been previously boiled for 10 min into the polyacrylamide gel at a final concentration of 10% (vol/vol).

We boiled 7.5 μL of protein samples with 2.5 μL 4× loading buffer (200 mM Tris-HCl, 8% [wt/vol] SDS, 40% [vol/vol] glycerol, trace bromophenol blue) for 10 min. We then electrophoresed these samples at 100 V for 4 h. All subsequent steps occurred with gentle rocking at ambient temperature unless otherwise noted. We washed the zymogram gel twice in 100 mL double-distilled water (ddH_2O) for 30 min. We then incubated the gel in 100 mL of renaturation buffer (20 mM Tris, 50 mM NaCl, 20 mM $MgCl_2$, 0.5% [vol/vol] Triton X-100 [pH 7.4]) for 1 h. After replacing the renaturation buffer with 100 mL fresh renaturation buffer, we incubated the zymogram for 12 h at 37°C. We stained the gel with 100 mL of staining solution (0.1% [wt/vol] methylene blue, 0.01% [wt/vol] KOH) for 1 h. We subsequently destained the gel with repeated washes in ddH_2O. We scored peptidoglycan degradation as zones of clearing within the stained gel (97).

Inhibition of *M. catarrhalis* using 6×His-SagA$^{37\text{-}197}$. We cultured *M. catarrhalis* strain O35E as above and diluted the culture to an OD_{600} of 0.01 in BHI. We then transferred 50 μL of culture into the wells of a 96-well plate containing either purified 6×His-SagA$^{37\text{-}197}$ or an equivalent purification from an *E. coli* strain Top10 culture harboring an empty pBAD30 vector as a negative control. We incubated the plate at 37°C in a microplate spectrophotometer (Biotek) with continuous orbital shaking for 13 h and measured the OD_{600} of each well at 1-h intervals.

ALI culture of airway epithelium. Human bronchial and tracheal epithelial cells were obtained from residual tissue from lungs destined for transplantation in collaboration with the UW Health Lung Transplant Program. The protocol was reviewed by the University of Wisconsin IRB and was deemed "not human subjects research." We thawed cryopreserved aliquots of cells and expanded them as monolayers in PneumaCult-Ex Plus Medium (StemCell Technologies) supplemented with 50 μg/mL gentamicin and 2 μg/mL fluconazole at 37°C in a 5% CO_2 atmosphere. Once the cells reached 80% confluence, we transferred them to 12-well plates with Transwell semipermeable inserts (Corning) and allowed them to differentiate in PneumaCult-ALI medium (StemCell Technologies) supplemented with gentamicin and fluconazole, as above, at the ALI until ciliary motion was observed (≥21 days). We cultured the cells in an antibiotic-free medium 48 h prior to bacterial inoculation.

Inhibition assays in airway epithelium cultures. We centrifuged liquid cultures of *R. aeria* strain RSM41, *R. dentocariosa* strain RSM522, and *R. similmucilaginosa* strain RSM42 at 5,000 × *g* for 5 min and resuspended the cell pellet to an OD_{600} of ~0.25 in prewarmed PBS. We cultured *M. catarrhalis* on BD Chocolate Agar–GC II Agar with IsoVitaleX and prepared a suspension of the bacterial cells to an OD_{600} of ~0.25 in prewarmed PBS. We inoculated the apical surface of separate wells of ALI cultures with 50

μL of a *Rothia* suspension for 40 h. We infected ALI cells with *M. catarrhalis* as previously described (98). Briefly, we infected the apical surface with 50 μL of the *M. catarrhalis* suspension and incubated the cells at 37°C for 24 h. At the end of the infection period, we gently washed the apical surface with 500 μL prewarmed PBS and collected the cells in 350 μL of RLT Plus Buffer (Qiagen) containing 0.5% Reagent DX (Qiagen).

Quantification of *M. catarrhalis* in airway epithelium cultures. We transferred the cells to PowerBead tubes (Qiagen) for bead beating (5 min, 50 oscillations/s, Qiagen TissueLyser LT). We then extracted RNA and DNA as separate fractions using the AllPrep DNA/RNA Minikit (Qiagen), following the manufacturer's instructions. We quantified *M. catarrhalis copB* DNA using real-time PCR on a 7500 Real Time PCR System (Applied Biosystems) using the specific primers *copB*-F (5′-GTGAGTGCCGCTTTACAACC-3′) and *copB*-R (5′-TGTATCGCCT GCCAAGACAA-3′), as previously described (99). We calibrated levels of *copB* to CFUe using a standard curve as previously described (98). Briefly, we cultured *M. catarrhalis* cultured overnight and quantified the CFU using standard methods. In parallel, we extracted DNA from an aliquot of the same culture using an AllPrep Power Viral kit (Qiagen) and prepared serial dilutions of the DNA corresponding to 10^2 to 10^6 CFU.

Statistical analysis and data visualization. All statistical analyses were performed in R with specific packages as described in the preceding sections. We generated graphics using ggplot2 (100) with some cleanup and assembly in InkScape.

Data availability. The raw amplicon sequences used for bacterial community analysis are deposited in the Short Read Archive under BioProject accession no. PRJNA866994. Genome sequences generated from this work are deposited under BioProject accession no. PRJNA867425. All other raw and derived data are available at https://doi.org/10.6084/m9.figshare.20444466. The scripts necessary to replicate this work are available at https://github.com/reedstubbendieck/rothia_moraxella.

SUPPLEMENTAL MATERIAL

Supplemental material is available online only.

FIG S1, TIF file, 0.3 MB.

FIG S2, TIF file, 0.3 MB.

FIG S3, TIF file, 4.8 MB.

FIG S4, TIF file, 1.3 MB.

FIG S5, TIF file, 0.5 MB.

TABLE S1, TXT file, 0 MB.

TABLE S2, TXT file, 0.04 MB.

TABLE S3, DOCX file, 0.01 MB.

ACKNOWLEDGMENTS

We thank Camila Carlos-Shanley (Texas State University) for assistance in amplicon sequencing. We thank Oliva Chao and Timothy Davenport (University of Wisconsin-Madison) for their assistance in culturing isolates for this project. We thank Timothy Murphy (The State University of New York) for the gift of *M. catarrhalis* strain O35E. We thank Rodney Welch (University of Wisconsin-Madison) for the gift of *E. coli* strain MG1665 and plasmid pBAD30. We thank Marc Chevrette (University of Florida) for comments on the manuscript.

This work, including the efforts of C.R.C., was funded by the National Institutes of Health Centers of Excellence for Translational Research (U19 AI142720). R.M.S. was supported by a National Library of Medicine training grant to the Computation and Informatics in Biology and Medicine Training Program (T15 LM007359) and startup funds from Oklahoma State University. S.E.Z. was supported by a National Institutes of Health National Research Service Award to the University of Wisconsin-Madison (TL1 TR002375). J.E.G., R.F.V., and the RhinoGen study were supported by the National Institute of Allergy and Infectious Diseases (U19 AI104317). The funders had no role in study design, data collection and interpretation, or the decision to submit the work for publication.

R.M.S., E.D., P.M.B., S.E.Z., J.E.G., and C.R.C. designed the research. R.M.S., E.D., P.M.B., S.E.Z., M.I.T., S.S.W., and R.F.V. performed the research. R.M.S., E.D., P.M.B., and S.E.Z. analyzed the data. R.M.S. generated the figures and wrote and revised the paper.

We declare that there are no conflicts of interest.

REFERENCES

1. Brugger SD, Bomar L, Lemon KP. 2016. Commensal-pathogen interactions along the human nasal passages. PLoS Pathog 12:e1005633. https://doi.org/10.1371/journal.ppat.1005633.
2. Bomar L, Brugger SD, Lemon KP. 2018. Bacterial microbiota of the nasal passages across the span of human life. Curr Opin Microbiol 41:8–14. https://doi.org/10.1016/j.mib.2017.10.023.

3. Escapa IF, Chen T, Huang Y, Gajare P, Dewhirst FE, Lemon KP. 2018. New insights into human nostril microbiome from the expanded Human Oral Microbiome Database (eHOMD): a resource for the microbiome of the human aerodigestive tract. mSystems 3:e00187-18. https://doi.org/10.1128/mSystems.00187-18.
4. Siegel SJ, Weiser JN. 2015. Mechanisms of bacterial colonization of the respiratory tract. Annu Rev Microbiol 69:425–444. https://doi.org/10.1146/annurev-micro-091014-104209.
5. von Eiff C, Becker K, Machka K, Stammer H, Peters G. 2001. Nasal carriage as a source of *Staphylococcus aureus* bacteremia. N Engl J Med 344:11–16. https://doi.org/10.1056/NEJM200101043440102.
6. Hsu HE, Shutt KA, Moore MR, Beall BW, Bennett NM, Craig AS, Farley MM, Jorgensen JH, Lexau CA, Petit S, Reingold A, Schaffner W, Thomas A, Whitney CG, Harrison LH. 2009. Effect of pneumococcal conjugate vaccine on pneumococcal meningitis. N Engl J Med 360:244–256. https://doi.org/10.1056/NEJMoa0800836.
7. Brown AO, Mann B, Gao G, Hankins JS, Humann J, Giardina J, Faverio P, Restrepo MI, Halade GV, Mortensen EM, Lindsey ML, Hanes M, Happel KI, Nelson S, Bagby GJ, Lorent JA, Cardinal P, Granados R, Esteban A, LeSaux CJ, Tuomanen EI, Orihuela CJ. 2014. *Streptococcus pneumoniae* translocates into the myocardium and forms unique microlesions that disrupt cardiac function. PLoS Pathog 10:e1004383. https://doi.org/10.1371/journal.ppat.1004383.
8. Muthukrishnan G, Lamers RP, Ellis A, Paramanandam V, Persaud AB, Tafur S, Parkinson CL, Cole AM. 2013. Longitudinal genetic analyses of *Staphylococcus aureus* nasal carriage dynamics in a diverse population. BMC Infect Dis 13:221. https://doi.org/10.1186/1471-2334-13-221.
9. Johnson HL, Deloria-Knoll M, Levine OS, Stoszek SK, Freimanis Hance L, Reithinger R, Muenz LR, O'Brien KL. 2010. Systematic evaluation of serotypes causing invasive pneumococcal disease among children under five: the pneumococcal global serotype project. PLoS Med 7:e1000348. https://doi.org/10.1371/journal.pmed.1000348.
10. Datta R, Shah A, Huang SS, Cui E, Nguyen V, Welbourne SJ, Quan KA, Thrupp L. 2014. High nasal burden of methicillin-resistant *Staphylococcus aureus* increases risk of invasive disease. J Clin Microbiol 52:312–314. https://doi.org/10.1128/JCM.01606-13.
11. Drijkoningen JJC, Rohde GGU. 2014. Pneumococcal infection in adults: burden of disease. Clin Microbiol Infect 20:45–51. https://doi.org/10.1111/1469-0691.12461.
12. Morrill HJ, Caffrey AR, Noh E, LaPlante KL. 2014. Epidemiology of pneumococcal disease in a national cohort of older adults. Infect Dis Ther 3:19–33. https://doi.org/10.1007/s40121-014-0025-y.
13. Tom S, Galbraith JC, Valiquette L, Jacobsson G, Collignon P, Schønheyder HC, Søgaard M, Kennedy KJ, Knudsen JD, Ostergaard C, Lyytikäinen O, Laupland KB, International Bacteraemia Surveillance Collaborative. 2014. Case fatality ratio and mortality rate trends of community-onset *Staphylococcus aureus* bacteraemia. Clin Microbiol Infect 20:O630–O632. https://doi.org/10.1111/1469-0691.12564.
14. Kaye KS, Petty LA, Shorr AF, Zilberberg MD. 2019. Current epidemiology, etiology, and burden of acute skin infections in the United States. Clin Infect Dis 68:S193–S199. https://doi.org/10.1093/cid/ciz002.
15. Murphy TF, Parameswaran GI. 2009. *Moraxella catarrhalis*, a human respiratory tract pathogen. Clin Infect Dis 49:124–131. https://doi.org/10.1086/599375.
16. Tong S, Amand C, Kieffer A, Kyaw MH. 2018. Trends in healthcare utilization and costs associated with acute otitis media in the United States during 2008–2014. BMC Health Serv Res 18:318. https://doi.org/10.1186/s12913-018-3139-1.
17. Pichichero M, Kaur R, Scott DA, Gruber WC, Trammel J, Almudevar A, Center KJ. 2018. Effectiveness of 13-valent pneumococcal conjugate vaccination for protection against acute otitis media caused by *Streptococcus pneumoniae* in healthy young children: a prospective observational study. Lancet Child Adolesc Health 2:561–568. https://doi.org/10.1016/S2352-4642(18)30168-8.
18. Bernhard S, Spaniol V, Aebi C. 2012. Molecular pathogenesis of infections caused by *Moraxella catarrhalis* in children. Swiss Med Wkly 142:w13694. https://doi.org/10.4414/smw.2012.13694.
19. Kaur R, Morris M, Pichichero ME. 2017. Epidemiology of acute otitis media in the postpneumococcal conjugate vaccine era. Pediatrics 140:e20170181. https://doi.org/10.1542/peds.2017-0181.
20. Wallace RJ, Steingrube VA, Nash DR, Hollis DG, Flanagan C, Brown BA, Labidi A, Weaver RE. 1989. BRO beta-lactamases of *Branhamella catarrhalis* and *Moraxella* subgenus *Moraxella*, including evidence for chromosomal beta-lactamase transfer by conjugation in *B. catarrhalis*, *M. nonliquefaciens*, and *M. lacunata*. Antimicrob Agents Chemother 33:1845–1854. https://doi.org/10.1128/AAC.33.11.1845.
21. Saito R, Nonaka S, Fujinami Y, Matsuoka S, Nakajima S, Nishiyama H, Okamura N. 2014. The frequency of BRO β-lactamase and its relationship to antimicrobial susceptibility and serum resistance in *Moraxella catarrhalis*. J Infect Chemother 20:6–8. https://doi.org/10.1016/j.jiac.2013.06.003.
22. Armbruster CE, Hong W, Pang B, Weimer KED, Juneau RA, Turner J, Swords WE. 2010. Indirect pathogenicity of *Haemophilus influenzae* and *Moraxella catarrhalis* in polymicrobial otitis media occurs via interspecies quorum signaling. mBio 1:e00102-10. https://doi.org/10.1128/mBio.00102-10.
23. Perez AC, Pang B, King LB, Tan L, Murrah KA, Reimche JL, Wren JT, Richardson SH, Ghandi U, Swords WE. 2014. Residence of *Streptococcus pneumoniae* and *Moraxella catarrhalis* within polymicrobial biofilm promotes antibiotic resistance and bacterial persistence *in vivo*. Pathog Dis 70:280–288. https://doi.org/10.1111/2049-632X.12129.
24. Bair KL, Campagnari AA. 2020. *Moraxella catarrhalis* promotes stable polymicrobial biofilms with the major otopathogens. Front Microbiol 10:3006. https://doi.org/10.3389/fmicb.2019.03006.
25. Kloepfer KM, Lee WM, Pappas TE, Kang TJ, Vrtis RF, Evans MD, Gangnon RE, Bochkov YA, Jackson DJ, Lemanske RF, Gern JE. 2014. Detection of pathogenic bacteria during rhinovirus infection is associated with increased respiratory symptoms and asthma exacerbations. J Allergy Clin Immunol 133:1301–1307. 1307.e1–1307.e3. https://doi.org/10.1016/j.jaci.2014.02.030.
26. Teo SM, Mok D, Pham K, Kusel M, Serralha M, Troy N, Holt BJ, Hales BJ, Walker ML, Hollams E, Bochkov YA, Grindle K, Johnston SL, Gern JE, Sly PD, Holt PG, Holt KE, Inouye M. 2015. The infant nasopharyngeal microbiome impacts severity of lower respiratory infection and risk of asthma development. Cell Host Microbe 17:704–715. https://doi.org/10.1016/j.chom.2015.03.008.
27. Tang HHF, Lang A, Teo SM, Judd LM, Gangnon R, Evans MD, Lee KE, Vrtis R, Holt PG, Lemanske RF, Jackson DJ, Holt KE, Inouye M, Gern JE. 2021. Developmental patterns in the nasopharyngeal microbiome during infancy are associated with asthma risk. J Allergy Clin Immunol 147:1683–1691. https://doi.org/10.1016/j.jaci.2020.10.009.
28. Verduin CM, Hol C, Fleer A, van Dijk H, van Belkum A. 2002. *Moraxella catarrhalis*: from emerging to established pathogen. Clin Microbiol Rev 15:125–144. https://doi.org/10.1128/CMR.15.1.125-144.2002.
29. Aebi C. 2011. *Moraxella catarrhalis*: pathogen or commensal? Adv Exp Med Biol 697:107–116. https://doi.org/10.1007/978-1-4419-7185-2_9.
30. Perez AC, Murphy TF. 2017. A *Moraxella catarrhalis* vaccine to protect against otitis media and exacerbations of COPD: an update on current progress and challenges. Hum Vaccin Immunother 13:2322–2331. https://doi.org/10.1080/21645515.2017.1356951.
31. De Smedt P, Leroux-Roels G, Vandermeulen C, Tasciotti A, Di Maro G, Dozot M, Casula D, Annaratone M, Riccucci D, Arora AK. 2021. Long-term immunogenicity and safety of a non-typeable *Haemophilus influenzae-Moraxella catarrhalis* vaccine: 4-year follow-up of a phase 1 multicentre trial. Vaccine X 9:100124. https://doi.org/10.1016/j.jvacx.2021.100124.
32. Andreas S, Testa M, Boyer L, Brusselle G, Janssens W, Kerwin E, Papi A, Pek B, Puente-Maestu L, Saralaya D, Watz H, Wilkinson TMA, Casula D, Di Maro G, Lattanzi M, Moraschini L, Schoonbroodt S, Tasciotti A, Arora AK, Maltais F, NTHi-Mcat-002 study group. 2022. Non-typeable *Haemophilus influenzae-Moraxella catarrhalis* vaccine for the prevention of exacerbations in chronic obstructive pulmonary disease: a multicentre, randomised, placebo-controlled, observer-blinded, proof-of-concept, phase 2b trial. Lancet Respir Med 10:435–446. https://doi.org/10.1016/S2213-2600(21)00502-6.
33. Galgani I, Annaratone M, Casula D, Di Maro G, Janssens M, Tasciotti A, Schwarz T, Ferguson M, Arora AK. 2022. Safety and immunogenicity of three doses of non-typeable *Haemophilus influenzae-Moraxella catarrhalis* (NTHi-Mcat) vaccine when administered according to two different schedules: a phase 2, randomised, observer-blind study. Respir Res 23:114. https://doi.org/10.1186/s12931-022-02019-4.
34. Cosgrove K, Coutts G, Jonsson I-M, Tarkowski A, Kokai-Kun JF, Mond JJ, Foster SJ. 2007. Catalase (KatA) and alkyl hydroperoxide reductase (AhpC) have compensatory roles in peroxide stress resistance and are required for survival, persistence, and nasal colonization in *Staphylococcus aureus*. J Bacteriol 189:1025–1035. https://doi.org/10.1128/JB.01524-06.
35. Krismer B, Liebeke M, Janek D, Nega M, Rautenberg M, Hornig G, Unger C, Weidenmaier C, Lalk M, Peschel A. 2014. Nutrient limitation governs *Staphylococcus aureus* metabolism and niche adaptation in the human nose. PLoS Pathog 10:e1003862. https://doi.org/10.1371/journal.ppat.1003862.

36. Hardy BL, Merrell DS. 2021. Friend or foe: interbacterial competition in the nasal cavity. J Bacteriol 203:e00480-20. https://doi.org/10.1128/JB.00480-20.
37. Stubbendieck RM, Straight PD. 2016. Multifaceted interfaces of bacterial competition. J Bacteriol 198:2145–2155. https://doi.org/10.1128/JB.00275-16.
38. Stubbendieck RM, May DS, Chevrette MG, Temkin MI, Wendt-Pienkowski E, Cagnazzo J, Carlson CM, Gern JE, Currie CR. 2019. Competition among nasal bacteria suggests a role for siderophore-mediated interactions in shaping the human nasal microbiota. Appl Environ Microbiol 85:e02046-18. https://doi.org/10.1128/AEM.02406-18.
39. Zipperer A, Konnerth MC, Laux C, Berscheid A, Janek D, Weidenmaier C, Burian M, Schilling NA, Slavetinsky C, Marschal M, Willmann M, Kalbacher H, Schittek B, Brötz-Oesterhelt H, Grond S, Peschel A, Krismer B. 2016. Human commensals producing a novel antibiotic impair pathogen colonization. Nature 535:511–516. https://doi.org/10.1038/nature18634.
40. Cole AL, Sundar M, Lopez A, Forsman A, Yooseph S, Cole AM. 2021. Identification of nasal *Gammaproteobacteria* with potent activity against *Staphylococcus aureus*: novel insights into the "noncarrier" state. mSphere 6:e01015-20. https://doi.org/10.1128/mSphere.01015-20.
41. Janek D, Zipperer A, Kulik A, Krismer B, Peschel A. 2016. High frequency and diversity of antimicrobial activities produced by nasal *Staphylococcus* strains against bacterial competitors. PLoS Pathog 12:e1005812. https://doi.org/10.1371/journal.ppat.1005812.
42. Bomar L, Brugger SD, Yost BH, Davies SS, Lemon KP. 2016. *Corynebacterium accolens* releases antipneumococcal free fatty acids from human nostril and skin surface triacylglycerols. mBio 7:e01725-15. https://doi.org/10.1128/mBio.01725-15.
43. Bashir H, Grindle K, Vrtis R, Vang F, Kang T, Salazar L, Anderson E, Pappas T, Gangnon R, Evans MD, Jackson DJ, Lemanske RF, Bochkov YA, Gern JE. 2018. Association of rhinovirus species with common cold and asthma symptoms and bacterial pathogens. J Allergy Clin Immunol 141:822–824.e9. https://doi.org/10.1016/j.jaci.2017.09.027.
44. Lemanske RF. 2002. The childhood origins of asthma (COAST) study. Pediatr Allergy Immunol 13:38–43. https://doi.org/10.1034/j.1399-3038.13.s.15.8.x.
45. Stoltz DJ, Jackson DJ, Evans MD, Gangnon RE, Tisler CJ, Gern JE, Lemanske RF. 2013. Specific patterns of allergic sensitization in early childhood and asthma & rhinitis risk. Clin Exp Allergy 43:233–241. https://doi.org/10.1111/cea.12050.
46. Richter M, Rosselló-Móra R. 2009. Shifting the genomic gold standard for the prokaryotic species definition. Proc Natl Acad Sci U S A 106:19126–19131. https://doi.org/10.1073/pnas.0906412106.
47. Donia MS, Cimermancic P, Schulze CJ, Wieland Brown LC, Martin J, Mitreva M, Clardy J, Linington RG, Fischbach MA. 2014. A systematic analysis of biosynthetic gene clusters in the human microbiome reveals a common family of antibiotics. Cell 158:1402–1414. https://doi.org/10.1016/j.cell.2014.08.032.
48. Aleti G, Baker JL, Tang X, Alvarez R, Dinis M, Tran NC, Melnik AV, Zhong C, Ernst M, Dorrestein PC, Edlund A. 2019. Identification of the bacterial biosynthetic gene clusters of the oral microbiome illuminates the unexplored social language of bacteria during health and disease. mBio 10:e00321-19. https://doi.org/10.1128/mBio.00321-19.
49. Stubbendieck RM, Zelasko SE, Safdar N, Currie CR. 2021. Biogeography of bacterial communities and specialized metabolism in human aerodigestive tract microbiomes. Microbiol Spectr 9:e01669-21. https://doi.org/10.1128/Spectrum.01669-21.
50. Blin K, Wolf T, Chevrette MG, Lu X, Schwalen CJ, Kautsar SA, Suarez Duran HG, de Los Santos ELC, Kim HU, Nave M, Dickschat JS, Mitchell DA, Shelest E, Breitling R, Takano E, Lee SY, Weber T, Medema MH. 2017. antiSMASH 4.0: improvements in chemistry prediction and gene cluster boundary identification. Nucleic Acids Res 45:W36–W41. https://doi.org/10.1093/nar/gkx319.
51. Uranga CC, Arroyo P, Duggan BM, Gerwick WH, Edlund A. 2020. Commensal oral *Rothia mucilaginosa* produces enterobactin, a metal-chelating siderophore. mSystems 5:e00161-20. https://doi.org/10.1128/mSystems.00161-20.
52. Winkelmann G. 2002. Microbial siderophore-mediated transport. Biochem Soc Trans 30:691–696. https://doi.org/10.1042/bst0300691.
53. Nambu T, Tsuzukibashi O, Uchibori S, Mashimo C. 2015. Complete genome sequence of *Rothia mucilaginosa* strain NUM-Rm6536, isolated from a human oral cavity. Genome Announc 3:e01122-15. https://doi.org/10.1128/genomeA.01122-15.
54. Anantharaman V, Aravind L. 2003. Evolutionary history, structural features and biochemical diversity of the NlpC/P60 superfamily of enzymes. Genome Biol 4:R11. https://doi.org/10.1186/gb-2003-4-2-r11.
55. Rawlings ND, Morton FR. 2008. The MEROPS batch BLAST: a tool to detect peptidases and their non-peptidase homologues in a genome. Biochimie 90:243–259. https://doi.org/10.1016/j.biochi.2007.09.014.
56. Sanchez-Pulido L, Ponting CP. 2016. Vasohibins: new transglutaminase-like cysteine proteases possessing a non-canonical Cys-His-Ser catalytic triad. Bioinforma Oxf Engl 32:1441–1445. https://doi.org/10.1093/bioinformatics/btv761.
57. Rosano GL, Ceccarelli EA. 2014. Recombinant protein expression in *Escherichia coli*: advances and challenges. Front Microbiol 5:172. https://doi.org/10.3389/fmicb.2014.00172.
58. Mark Welch JL, Rossetti BJ, Rieken CW, Dewhirst FE, Borisy GG. 2016. Biogeography of a human oral microbiome at the micron scale. Proc Natl Acad Sci U S A 113:E791–800. https://doi.org/10.1073/pnas.1522149113.
59. Oishi T, Muratani T, Tanaka T, Sato M, Kohdera U, Ouchi K, Iwata S, Matsumoto T, Nakahama C. 2021. Study of normal flora in the pharynx of healthy children. Jpn J Infect Dis 74:450–457. https://doi.org/10.7883/yoken.JJID.2020.824.
60. Laufer AS, Metlay JP, Gent JF, Fennie KP, Kong Y, Pettigrew MM. 2011. Microbial communities of the upper respiratory tract and otitis media in children. mBio 2:e00245-10. https://doi.org/10.1128/mBio.00245-10.
61. Wang H, Dai W, Feng X, Zhou Q, Wang H, Yang Y, Li S, Zheng Y. 2018. Microbiota composition in upper respiratory tracts of healthy children in Shenzhen, China, differed with respiratory sites and ages. Biomed Res Int 2018:6515670. https://doi.org/10.1155/2018/6515670.
62. Chen C-H, Liou M-L, Lee C-Y, Chang M-C, Kuo H-Y, Chang T-H. 2019. Diversity of nasal microbiota and its interaction with surface microbiota among residents in healthcare institutes. Sci Rep 9:6175. https://doi.org/10.1038/s41598-019-42548-5.
63. Fatahi-Bafghi M. 2021. Characterization of the *Rothia* spp. and their role in human clinical infections. Infect Genet Evol 93:104877. https://doi.org/10.1016/j.meegid.2021.104877.
64. Rigauts C, Aizawa J, Taylor SL, Rogers GB, Govaerts M, Cos P, Ostyn L, Sims S, Vandeplassche E, Sze M, Dondelinger Y, Vereecke L, Van Acker H, Simpson JL, Burr L, Willems A, Tunney MM, Cigana C, Bragonzi A, Coenye T, Crabbé A. 2022. *Rothia mucilaginosa* is an anti-inflammatory bacterium in the respiratory tract of patients with chronic lung disease. Eur Respir J 59:2101293. https://doi.org/10.1183/13993003.01293-2021.
65. Griffin ME, Espinosa J, Becker JL, Luo J-D, Carroll TS, Jha JK, Fanger GR, Hang HC. 2021. *Enterococcus* peptidoglycan remodeling promotes checkpoint inhibitor cancer immunotherapy. Science 373:1040–1046. https://doi.org/10.1126/science.abc9113.
66. Lee J, Leichtle A, Zuckerman E, Pak K, Spriggs M, Wasserman SI, Kurabi A. 2019. NOD1/NOD2-mediated recognition of non-typeable *Haemophilus influenzae* activates innate immunity during otitis media. Innate Immun 25:503–512. https://doi.org/10.1177/1753425919872266.
67. Berrington WR, Iyer R, Wells RD, Smith KD, Skerrett SJ, Hawn TR. 2010. NOD1 and NOD2 regulation of pulmonary innate immunity to *Legionella pneumophila*. Eur J Immunol 40:3519–3527. https://doi.org/10.1002/eji.201040518.
68. Kale SD, Dikshit N, Kumar P, Balamuralidhar V, Khameneh HJ, Bin Abdul Malik N, Koh TH, Tan GGY, Tan TT, Mortellaro A, Sukumaran B. 2017. Nod2 is required for the early innate immune clearance of *Acinetobacter baumannii* from the lungs. Sci Rep 7:17429. https://doi.org/10.1038/s41598-017-17653-y.
69. Lee H-Y, Andalibi A, Webster P, Moon S-K, Teufert K, Kang S-H, Li J-D, Nagura M, Ganz T, Lim DJ. 2004. Antimicrobial activity of innate immune molecules against *Streptococcus pneumoniae*, *Moraxella catarrhalis* and nontypeable *Haemophilus influenzae*. BMC Infect Dis 4:12. https://doi.org/10.1186/1471-2334-4-12.
70. Ferraboschi P, Ciceri S, Grisenti P. 2021. Applications of lysozyme, an innate immune defense factor, as an alternative antibiotic. Antibiotics 10:1534. https://doi.org/10.3390/antibiotics10121534.
71. Ellison RT, Giehl TJ, LaForce FM. 1988. Damage of the outer membrane of enteric Gram-negative bacteria by lactoferrin and transferrin. Infect Immun 56:2774–2781. https://doi.org/10.1128/iai.56.11.2774-2781.1988.
72. Raphael GD, Jeney EV, Baraniuk JN, Kim I, Meredith SD, Kaliner MA. 1989. Pathophysiology of rhinitis. Lactoferrin and lysozyme in nasal secretions. J Clin Invest 84:1528–1535. https://doi.org/10.1172/JCI114329.
73. Chen S, Zhou Y, Chen Y, Gu J. 2018. Fastp: an ultra-fast all-in-one FASTQ preprocessor. Bioinformatics 34:i884–i890. https://doi.org/10.1093/bioinformatics/bty560.
74. Schloss PD, Westcott SL, Ryabin T, Hall JR, Hartmann M, Hollister EB, Lesniewski RA, Oakley BB, Parks DH, Robinson CJ, Sahl JW, Stres B, Thallinger GG, Van Horn DJ, Weber CF. 2009. Introducing mothur: open-source, platform-independent, community-supported software for describing and

comparing microbial communities. Appl Environ Microbiol 75:7537–7541. https://doi.org/10.1128/AEM.01541-09.
75. R Core Team. 2018. R: a language and environment for statistical computing. R Foundation for Statistical Computing, Vienna, Austria.
76. McMurdie PJ, Holmes S. 2013. phyloseq: an R package for reproducible interactive analysis and graphics of microbiome census data. PLoS One 8:e61217. https://doi.org/10.1371/journal.pone.0061217.
77. Oksanen J, Blanchet FG, Friendly M, Kindt R, Legendre P, McGlinn D, Minchin PR, O'Hara RB, Simpson GL, Solymos P, Stevens MHH, Szoecs E, Wagner H. 2019. vegan: community Ecology Package. https://CRAN.R-project.org/package=vegan.
78. Frank JA, Reich CI, Sharma S, Weisbaum JS, Wilson BA, Olsen GJ. 2008. Critical evaluation of two primers commonly used for amplification of bacterial 16S rRNA genes. Appl Environ Microbiol 74:2461–2470. https://doi.org/10.1128/AEM.02272-07.
79. Wang Q, Garrity GM, Tiedje JM, Cole JR. 2007. Naive Bayesian classifier for rapid assignment of rRNA sequences into the new bacterial taxonomy. Appl Environ Microbiol 73:5261–5267. https://doi.org/10.1128/AEM.00062-07.
80. Bankevich A, Nurk S, Antipov D, Gurevich AA, Dvorkin M, Kulikov AS, Lesin VM, Nikolenko SI, Pham S, Prjibelski AD, Pyshkin AV, Sirotkin AV, Vyahhi N, Tesler G, Alekseyev MA, Pevzner PA. 2012. SPAdes: a new genome assembly algorithm and its applications to single-cell sequencing. J Comput Biol J Comput Mol Cell Biol 19:455–477. https://doi.org/10.1089/cmb.2012.0021.
81. Seemann T. 2014. Prokka: rapid prokaryotic genome annotation. Bioinformatics 30:2068–2069. https://doi.org/10.1093/bioinformatics/btu153.
82. Melnyk RA, Hossain SS, Haney CH. 2019. Convergent gain and loss of genomic islands drive lifestyle changes in plant-associated *Pseudomonas*. ISME J 13:1575–1588. https://doi.org/10.1038/s41396-019-0372-5.
83. Almagro Armenteros JJ, Tsirigos KD, Sønderby CK, Petersen TN, Winther O, Brunak S, von Heijne G, Nielsen H. 2019. SignalP 5.0 improves signal peptide predictions using deep neural networks. Nat Biotechnol 37:420–423. https://doi.org/10.1038/s41587-019-0036-z.
84. Eren AM, Kiefl E, Shaiber A, Veseli I, Miller SE, Schechter MS, Fink I, Pan JN, Yousef M, Fogarty EC, Trigodet F, Watson AR, Esen ÖC, Moore RM, Clayssen Q, Lee MD, Kivenson V, Graham ED, Merrill BD, Karkman A, Blankenberg D, Eppley JM, Sjödin A, Scott JJ, Vázquez-Campos X, McKay LJ, McDaniel EA, Stevens SLR, Anderson RE, Fuessel J, Fernandez-Guerra A, Maignien L, Delmont TO, Willis AD. 2020. Community-led, integrated, reproducible multi-omics with anvi'o. Nat Microbiol 6:3–6. https://doi.org/10.1038/s41564-020-00834-3.
85. Chevrette MG, Currie CR. 2018. Emerging evolutionary paradigms in antibiotic discovery. J Ind Microbiol Biotechnol 46:257–271. https://doi.org/10.1007/s10295-018-2085-6.
86. Navarro-Muñoz JC, Selem-Mojica N, Mullowney MW, Kautsar SA, Tryon JH, Parkinson EI, De Los Santos ELC, Yeong M, Cruz-Morales P, Abubucker S, Roeters A, Lokhorst W, Fernandez-Guerra A, Cappelini LTD, Goering AW, Thomson RJ, Metcalf WW, Kelleher NL, Barona-Gomez F, Medema MH. 2020. A computational framework to explore large-scale biosynthetic diversity. Nat Chem Biol 16:60–68. https://doi.org/10.1038/s41589-019-0400-9.
87. Pérez-Miranda S, Cabirol N, George-Téllez R, Zamudio-Rivera LS, Fernández FJ. 2007. O-CAS, a fast and universal method for siderophore detection. J Microbiol Methods 70:127–131. https://doi.org/10.1016/j.mimet.2007.03.023.
88. Yoon S, Dispirito AA, Kraemer SM, Semrau JD. 2011. A simple assay for screening microorganisms for chalkophore production. Methods Enzymol 495:247–258. https://doi.org/10.1016/B978-0-12-386905-0.00016-4.
89. Schwyn B, Neilands JB. 1987. Universal chemical assay for the detection and determination of siderophores. Anal Biochem 160:47–56. https://doi.org/10.1016/0003-2697(87)90612-9.
90. Hoefler BC, Gorzelnik KV, Yang JY, Hendricks N, Dorrestein PC, Straight PD. 2012. Enzymatic resistance to the lipopeptide surfactin as identified through imaging mass spectrometry of bacterial competition. Proc Natl Acad Sci U S A 109:13082–13087. https://doi.org/10.1073/pnas.1205586109.
91. Nesvizhskii AI, Keller A, Kolker E, Aebersold R. 2003. A statistical model for identifying proteins by tandem mass spectrometry. Anal Chem 75:4646–4658. https://doi.org/10.1021/ac0341261.
92. Kumar S, Stecher G, Li M, Knyaz C, Tamura K. 2018. MEGA X: Molecular Evolutionary Genetics Analysis across computing platforms. Mol Biol Evol 35:1547–1549. https://doi.org/10.1093/molbev/msy096.
93. Zhou L, Feng T, Xu S, Gao F, Lam TT, Wang Q, Wu T, Huang H, Zhan L, Li L, Guan Y, Dai Z, Yu G. 2022. ggmsa: A visual exploration tool for multiple sequence alignment and associated data. Brief Bioinform 23:bbac222. https://doi.org/10.1093/bib/bbac222.
94. Kelley LA, Mezulis S, Yates CM, Wass MN, Sternberg MJE. 2015. The Phyre2 web portal for protein modeling, prediction and analysis. Nat Protoc 10:845–858. https://doi.org/10.1038/nprot.2015.053.
95. Schrödinger. The PyMOL molecular graphics system. Version 2.5.0. Schrödinger, New York, NY. https://pymol.org/2/.
96. Gibson DG, Young L, Chuang R-Y, Venter JC, Hutchison CA, Smith HO. 2009. Enzymatic assembly of DNA molecules up to several hundred kilobases. Nat Methods 6:343–345. https://doi.org/10.1038/nmeth.1318.
97. Dufour D, Lévesque C. 2013. Zymogram assay for the detection of peptidoglycan hydrolases in *Streptococcus mutans*. BIO-Protoc 3. https://doi.org/10.21769/BioProtoc.855.
98. Dissanayake E, Brockman-Schneider RA, Stubbendieck RM, Helling BA, Zhang Z, Bochkov YA, Kirkham C, Murphy TF, Ober C, Currie CR, Gern JE. 2023. Rhinovirus increases *Moraxella catarrhalis* adhesion to the respiratory epithelium. Front Cell Infect Microbiol 12:1060748. https://doi.org/10.3389/fcimb.2022.1060748.
99. Greiner O, Day PJR, Altwegg M, Nadal D. 2003. Quantitative detection of *Moraxella catarrhalis* in nasopharyngeal secretions by real-time PCR. J Clin Microbiol 41:1386–1390. https://doi.org/10.1128/JCM.41.4.1386-1390.2003.
100. Wickham H. 2016. ggplot2: Elegant graphics for data analysis. Available from https://ggplot2.tidyverse.org/. Springer-Verlag New York, New York, NY.